

Article

Investigating the Relationship between Precipitation and Vegetation Dynamics with Emphasis on Agricultural Land Cover in the Atrak Basin Area

Iman Rousta ^{1,2} , Fatemeh Shakiba ¹, Haraldur Olafsson ², Edgar Ricardo Monroy Vargas ³, Anna Siedliska ⁴ 
and Jaromir Krzyszczyk ^{4,*} 

¹ Department of Geography, Yazd University, Yazd P.O. Box 8915818411, Iran; irousta@yazd.ac.ir (I.R.); f.shakiba@stu.yazd.ac.ir (F.S.)

² Institute for Atmospheric Sciences, Weather and Climate and Department of Physics, University of Iceland and Icelandic Meteorological Office (IMO), Bustadavegur 7, IS-108 Reykjavik, Iceland; haraldur@hi.is

³ Department of Engineering, Rosario University, Bogota 11011, Colombia; vanrodriguez@uan.edu.co

⁴ Institute of Agrophysics, Polish Academy of Sciences, Doświadczalna 4, 20-290 Lublin, Poland; a.siedliska@ipan.lublin.pl

* Correspondence: j.krzyszczyk@ipan.lublin.pl

Abstract: The present study aimed to analyze the dynamics of vegetation within the Atrak catchment area, as well as its interplay with precipitation patterns. Moreover, additional emphasis was placed on exploring the impact of these dynamics on agricultural land cover type. To achieve this objective, the Enhanced Vegetation Index (EVI) derived from MODIS data and the Comprehensive Historical and Real-Time Satellite-based Precipitation (CHRIPS) data were utilized for the period from 2003 to 2021. Additionally, the Vegetation Condition Index (VCI) and Standardized Precipitation Index (SPI) were employed to discern various degrees of drought and pluvial years within the Atrak basin. The study revealed that the years 2008, 2014, 2017, and 2021 exhibited the lowest vegetation coverage, while the years 2010, 2016, and 2019 showcased the most extensive vegetation extent. Notably, it was revealed from the VCI index that the year 2008 was the driest, and the year 2016 was the wettest. Furthermore, based on the SPI index findings, the years 2007, 2019, and 2020 were identified as pluvial years, while in the years 2008, 2014, and 2021 drought conditions occurred. All other years were classified as exhibiting normal conditions. Regarding seasonality, the observations ascertain that the spring season substantiates the most extensive vegetation cover, and a high correlation between spring precipitation and vegetation coverage was observed. Additionally, the anomaly detection outcomes indicate that the eastern regions of the basin have experienced an upward trend compared to the average of the first decade of the studied period.

Keywords: vegetation; agricultural lands; precipitation; remote sensing; Atrak watershed



Citation: Rousta, I.; Shakiba, F.; Olafsson, H.; Vargas, E.R.M.; Siedliska, A.; Krzyszczyk, J. Investigating the Relationship between Precipitation and Vegetation Dynamics with Emphasis on Agricultural Land Cover in the Atrak Basin Area. *Atmosphere* **2024**, *15*, 489. <https://doi.org/10.3390/atmos15040489>

Academic Editor: Giacomo Alessandro Gerosa

Received: 3 February 2024

Revised: 19 March 2024

Accepted: 13 April 2024

Published: 15 April 2024



Copyright: © 2024 by the authors. Licensee MDPI, Basel, Switzerland. This article is an open access article distributed under the terms and conditions of the Creative Commons Attribution (CC BY) license (<https://creativecommons.org/licenses/by/4.0/>).

1. Introduction

The exploration of topics such as sustainable vegetation management and control encompasses a pivotal concern within ecological research, specifically those studies delving into the sustainable processes governing vegetation fluctuations [1]. Given the significance of climate change in contemporary discourse, significant efforts are dedicated to investigating the impact of meteorological factors on vegetation dynamics [2]. The study of changes in vegetation patterns serves as an indicator of the dynamism of ecosystems, thereby allowing for their management to uphold ecosystem stability [3]. Numerous natural and anthropogenic factors, including climate change, lead to changes in various phenomena and effects occurring on the Earth's surface, including vegetation growth [4]. The pivotal role of vegetation in supplying organic matter, regulating the carbon cycle, and facilitating energy exchanges in response to climatic changes underscores the need to discern, predict,

and proactively address such ecosystem changes [5–7]. Climatic characteristics exert a profound influence on various environmental parameters. The interplay between vegetation and climate exhibits a robust correlation, with alterations in either entity resulting in repercussions for other ecological functions. Precipitation amount, timing, frequency, spatial distribution, and intensity, alongside temperature regimes, intermingle with topographical features to bestow distinct vegetation patterns in different geographical regions [8].

The geographical distribution of different plant communities depends heavily on prevailing climatic conditions, to the extent that climate represents a preeminent determinant of vegetation characteristics on both local and global scales. Among climatic variables, temperature and precipitation have the most significant impact on the spatiotemporal patterns of vegetation [9,10]. Drought, stemming from climate shifts and perturbations in atmospheric circulation, emerges as a primary contributor to vegetation reduction. Given the pivotal role that rainfall plays in both the growth and degradation of vegetation, the reduction in vegetation is directly linked to insufficient rainfall. Moreover, when accompanied by elevated air temperatures, strong winds, and reduced relative humidity, this combination exacerbates drought conditions and, conversely, diminishes the intensity of green cover [11]. Vegetation is known to be a widely used biome in ecological assessments due to such characteristics as immobility, or relatively rapid growth. The increase in vegetation cover in an area reduces atmospheric carbon dioxide [12], mitigates lead concentrations, regulates soil moisture, safeguards water resources [13,14], curtails soil erosion, and diminishes flood risks, thereby contributing to ecological sustainability [15,16]. While in some regions droughts are the main problem, in others flooding takes place [17]. Consequently, environmental instability is liable to manifest as desertification, soil erosion, climate perturbations, and other effects, heralding adverse economic, societal, and climatic consequences [18].

A series of scientific studies have explored the dynamics of plant growth in various geographical regions, employing sophisticated methodologies and data sources. For instance, the changes in the vegetation cover in Fars province were investigated by utilizing the NDVI index and the Mann–Kendall test [19]. These investigations revealed a consistent increase in the rate of plant growth in mountainous regions compared to plain areas. In another study, satellite data were utilized in conjunction with time series regression analysis to examine the relationship between drought and vegetation in Afghanistan [20]. The outcomes of this study indicated that in 2009 and 2010, there was a significant increase in vegetation cover, amounting to 16.3%. This increase was attributed in part to lower temperatures and greater precipitation compared to preceding years. MODIS NDVI and ERA-5 temperature and precipitation datasets were used to scrutinize spatial and temporal transformations in NDVI [21], and the responses of vegetation to climate alterations were analyzed using regression models and Pearson correlation coefficients. Furthermore, NDVI MODIS data were used and the stability and regression analysis methodologies were employed to explore spatiotemporal variations in vegetation cover within the Pearl River Delta from 2000 to 2015 [22]. The findings highlighted an upward trend in vegetation cover over this period, revealing a discernible correlation between changes in city-adjacent vegetation and human activities.

The impact of climatic elements such as temperature, precipitation, and drought on shifts in both linear and non-linear trends of vegetation cover was also investigated [23]. This study was conducted for the Khor-Sifiderak watershed within the Alborz province and employed satellite images spanning from 2000 to 2019. Results indicated a lack of a significant trend in regional precipitation over the two decades, while temperature exhibited a noteworthy declining trend. The influence of drought on vegetation was evident, with the most pronounced decline observed in 2008 due to severe drought conditions.

In an endeavor to comprehend the sustainability of vegetative fluctuations in the northern catchment of Afghanistan, MODIS data were harnessed in conjunction with rainfall records (PDIRNOW) [18]. The analysis revealed that the mean vegetation coverage throughout the entire period was 45.21%. The lowest levels of vegetation coverage were

observed during the 2001–2008 period and 2011, attributed to scarce rainfall. Conversely, in the years 2003, 2009, and 2010, increased precipitation alongside lower land surface temperature (LST) corresponded to the peak of vegetation coverage. Through the application of a structural equation model, the intricate relationship between driving factors and variations in the Enhanced Vegetation Index (EVI) in Anhui, China, from 2000 to 2020 was investigated [24]. The authors' holistic analysis unveiled that EVI transformations were predominantly steered by urbanization. Human activities significantly affected changes in central and southern Anhui, with subsequent pronounced feedback in EVI alterations due to annual rainfall fluctuations. Topographical factors exerted both direct and indirect impacts on changes in the northern and central regions compared to their southern counterpart. Conversely, alterations in annual temperature exerted minimal influence on the vegetation across the entire region.

The non-parametric methodology proposed by Mann–Kendall was utilized in conjunction with remote sensing and used to scrutinize the trend trajectory of vegetation alterations within northeastern Iran from 2000 to 2018 [5]. The results underscored that 52% of the studied area exhibited a declining vegetation trend, while the remaining regions demonstrated an ascending trend. Remote sensing data were used to investigate changes in vegetation cover and weather patterns in the Kabul River Basin in Afghanistan during the period 2001–2019 [25]. The results showed that precipitation and land surface temperature are influential factors in the vegetation cover of this region, with land surface temperature playing a more prominent role in winter. Weather patterns can serve as a warning system to prevent water or temperature stress in agricultural areas [26].

The relationship between climatic parameters and vegetation cover changes in the watersheds of the Caspian Sea was investigated using satellite images from 2001 to 2019 [27]. The results revealed that precipitation had little effect on vegetation cover during winter, but was the main controlling factor of vegetation cover in spring. In summer, the surface temperature was identified as the primary factor influencing vegetation cover.

The spatiotemporal characteristics of vegetation cover in the Middle East between 2001 and 2019 were analyzed using the NDVI [28]. The results indicate an increase in vegetation cover in the Middle East, particularly in Egypt and Saudi Arabia, with government policies being the main reason behind this. Additionally, both vegetation cover and density have increased in Turkey, which can be attributed to the construction of dams such as Ataturk and Ilisu. The impact of vegetation cover, land surface temperature, and precipitation on changes in water level and area of seven inland lakes in the Middle East area from 2000 to 2019 were investigated using elevation data [29]. The study focused on Urmia Lake in Iran, Mosul and Hamar 4 Lagoon in Iraq, and Bishahir and Archak Lakes in Turkey. The results revealed an increase in vegetation cover and land surface temperature, and a decrease in annual precipitation in the assessed area. Changes in temperature and vegetation cover were similar in all three countries, but changes in water levels and the lake areas were influenced by factors other than climate and varied significantly. Notably, Lake Urmia exhibited the most pronounced reduction in water levels.

In another recent study, the remote sensing data from the MODIS-GPM and GLADAS satellites were utilized to investigate the complex relationship between meteorological parameters, drought conditions, and vegetation diversity within the eastern basins of Afghanistan [30]. Employing regression methods, it was found that certain years, namely 2000, 2001, and 2008, displayed diminished vegetation cover, while the years 2010, 2013, 2016, and 2020 exhibited heightened levels of vegetation cover, accompanied by an ascending trend in the whole period. Overall, changes in soil moisture, precipitation, surface temperature, and the presence of drought conditions collectively accounted for 45% of the annual variations in vegetation cover.

However, there is still a need to assess how meteorological conditions influence the vegetation in various areas of the world. The Atrak Basin faces challenges related to water scarcity due to increasing demand from various sectors such as agriculture, industry, and domestic use. Climate change exacerbates these issues by altering precipitation pat-

terns and increasing evaporation rates. Research is needed to develop sustainable water management strategies [26,31], including efficient irrigation techniques, water recycling, and groundwater recharge methods. Intensive agricultural practices, deforestation, and overgrazing contribute to soil erosion and degradation in the Atrak Basin. This diminishes soil fertility, reduces agricultural productivity, and increases the risk of desertification. Scientists are exploring soil conservation measures, such as terracing, reforestation, and sustainable grazing practices, to mitigate these impacts. Therefore, the main aim of this research was to contribute to a comprehensive understanding of the interplay between rainfall patterns and the dynamics of vegetation within the Atrak basin area. Notably, the Atrak basin, the focal point of the present study, represents one of the longest rivers within Iran and forms a subunit of the broader Mazandaran Sea basin. This study analyzed the relationship between vegetation cover and drought conditions, quantified through the Vegetation Condition Index (VCI) and the Standardized Precipitation Index (SPI). It aimed to identify the impact of precipitation variability on vegetation cover and drought occurrence while examining changes in agricultural land coverage within the Atrak basin over the study period. The paper is organized as follows: after the introduction, the study area is described, followed by a presentation of the data sources and their features. The methods used are then described. Subsequently, the obtained results are presented and discussed, leading to the conclusion of the paper.

2. Materials and Methods

2.1. Study Area

The Atrak basin is classified as an open basin within Iran, and it holds the status of being a sub-basin in the broader framework of Iran's basin divisions. This particular basin is categorized as a sub-entity within the Mazandaran Sea basin area. Situated in the northeastern region of the country and positioned in the northern part of Khorasan province, its geographical coordinates span from 54° to 59°4' E and 38°57' to 38°17' N. Geographically, this basin shares borders with multiple entities: the Republic of Turkmenistan to the north, the Gorgan River basin and the Kal Shur (central desert) to the south, the Qara Qom basin to the east, and the Mazandaran Sea to the west. Excluding the portion situated in Turkmenistan, the overall expanse of the Atrak basin accounts for approximately 25,627 km². A significant portion of this basin is located within the provinces of North Khorasan and the northern region of Razavi Khorasan, encompassing an area spanning about 19,075 km². The principal river traversing this basin stretches approximately 520 km in length, and its primary trajectory extends from east to west, ultimately terminating at the Caspian Sea. The elevation of the Atrak River basin varies significantly, ranging from approximately 2903 m upstream to −22 m in coastal areas near the Caspian Sea. The landscape consists predominantly of mountains and plains, with mountains covering 5.76% of the area and plains encompassing 95.23% (Figure 1). The Atrak basin climate is marked by semi-arid conditions and notable variability. Due to its mountainous terrain, the distribution of rainfall across the Atrak basin showcases pronounced spatial fluctuations, with rainfall ranging from approximately 200 mm in the northwestern regions to 750 mm in mountainous areas. However, a significant portion of the watershed receives between 250 and 400 mm of precipitation. On the other hand, distinct seasonal variations in rainfall are also observed, typically concentrated during the winter and spring months.

Primary crops cultivated in the Atrak Basin include winter wheat (*Triticum aestivum* L.), barley (*Hordeum vulgare*), alfalfa (*Medicago sativa*), and various fodder crops essential for livestock husbandry. These crops are strategically planted to capitalize on seasonal rainfall patterns, with winter wheat being a prominent staple due to its resilience to the region's climatic conditions. In addition to rainfed agriculture, irrigation plays a crucial role in enhancing agricultural productivity, particularly in areas where water scarcity poses challenges to traditional farming practices. The basin hosts several irrigation schemes and cultivated areas where water resources are managed to support crop cultivation throughout

the year. The agricultural lands of the region amount to 147,521 ha, of which 74% is rainfed, and the remaining 26% is irrigated.

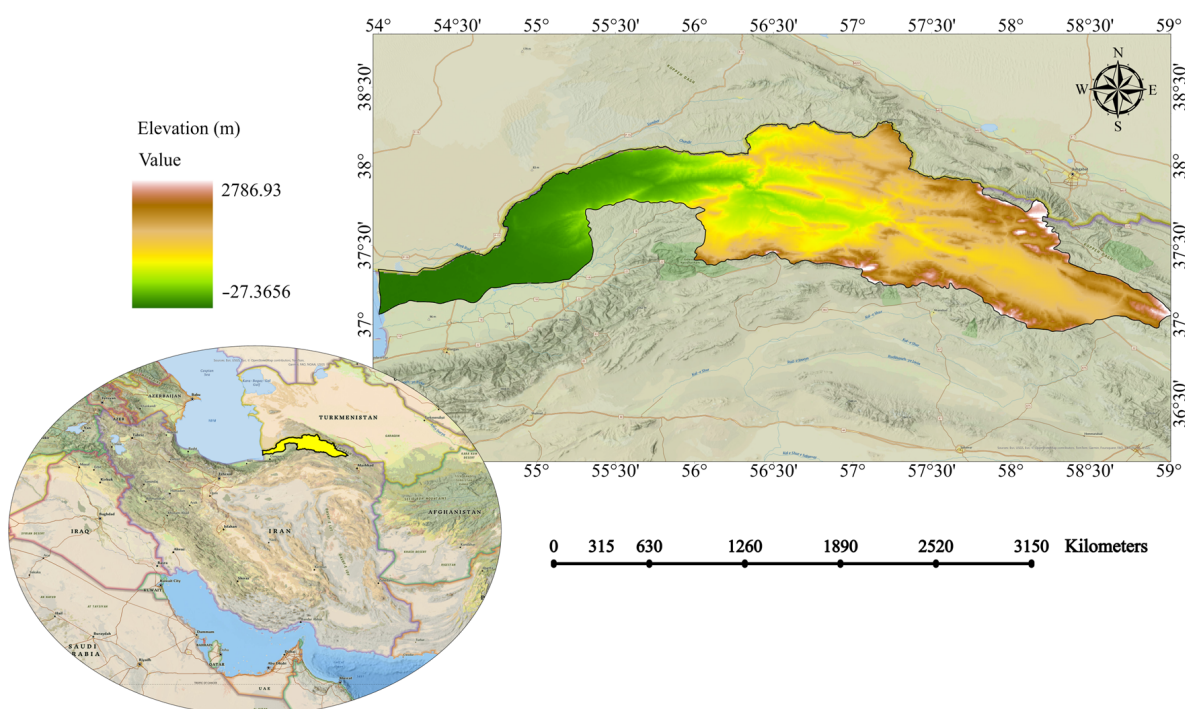


Figure 1. Maps showing the location of the Atrak basin in Iran and its orography.

Grassland ecosystems support a rich diversity of grass species and herbaceous vegetation. These ecosystems are vital for grazing livestock, conserving soil moisture, and sustaining biodiversity within the region. Various pasture plants are found in this area, with the primary type being darme (*Astragalus* spp.). Additionally, other species such as goon (*Ferula* spp.), ferion (*Euphorbia rigida*), saltgrass (*Distichlis spicata*), Iranian grass (*Agropyron cristatum*), stipa (*Stipa* spp.), *Poa* spp., *Festuca* spp., and *Aegilops* spp., among others, constitute key elements of the pastures in this region [32]. These grasses are well-adapted to the semi-arid conditions of the basin, exhibiting traits such as deep root systems, drought tolerance, and efficient water use efficiency. Grasslands in the Atrak Basin typically display varying degrees of vegetation cover, influenced by factors such as precipitation patterns, soil fertility, and grazing pressure. In areas with adequate moisture, dense stands of grasses may form extensive carpets of greenery, providing valuable forage for livestock and wildlife. However, in more arid regions, grassland vegetation cover may be sparse, with patches of bare soil interspersed between tufts of grass. Like shrublands, grasslands are susceptible to desertification when subjected to unsustainable land management practices and environmental stressors. Overgrazing, soil erosion, and habitat fragmentation can contribute to the degradation of grassland ecosystems, leading to loss of biodiversity and decreased productivity. Implementing holistic land management strategies, such as rotational grazing and reforestation, can help mitigate the threat of desertification and promote the resilience of grassland habitats. Grasslands cover 60% of the area of the watershed.

The shrubland ecosystems within the Atrak Basin are dominated by xerophytic shrubs and drought-resistant vegetation. These ecosystems play a crucial role in stabilizing soil, conserving water, and providing a habitat for a diverse array of flora and fauna. Common shrub species found in the shrublands of the Atrak Basin include *Artemisia* spp. (such as *Artemisia aucheri* and *Artemisia sieberi*), *Zygophyllum* spp., *Salsola* spp., and *Haloxylon* spp. These shrubs are adapted to arid conditions, featuring deep root systems to access water stored in the soil and mechanisms to minimize water loss through transpiration. Shrublands are particularly vulnerable to desertification, a process exacerbated by factors such as

overgrazing, deforestation, and unsustainable land management practices. In the Atrak Basin, the encroachment of desertification threatens to degrade shrubland ecosystems, leading to soil erosion, loss of biodiversity, and reduced ecosystem resilience. Effective land conservation and restoration measures are essential to mitigate the impacts of desertification and preserve the ecological integrity of shrubland habitats [33].

The rest of the lands of the Atrak watershed are residential, barren, marshy, and salt marshy areas [34].

The land cover map of the Atrak basin, based on the classification scheme developed by the University of Maryland [35] that divides land use into 17 distinct types [36], was extracted from the website of the United States government (<https://earthexplorer.usgs.gov/> (accessed on 10 July 2023)). The land cover map of the Atrak basin was divided into 6 distinct classes, 0, 7, 10, 12, 13, and 15 using the MODIS Land Cover Type (MCD12Q1) product, which provides global land cover maps with a 500 m spatial view and annual output [37–39]. According to Figure 2, the Atrak basin includes water areas, open shrublands, grasslands, croplands, and urban and non-vegetated land. A large part of the basin consists of grasslands, concentrated mostly in the central and eastern areas, while the western parts of the basin are characterized by open shrublands.

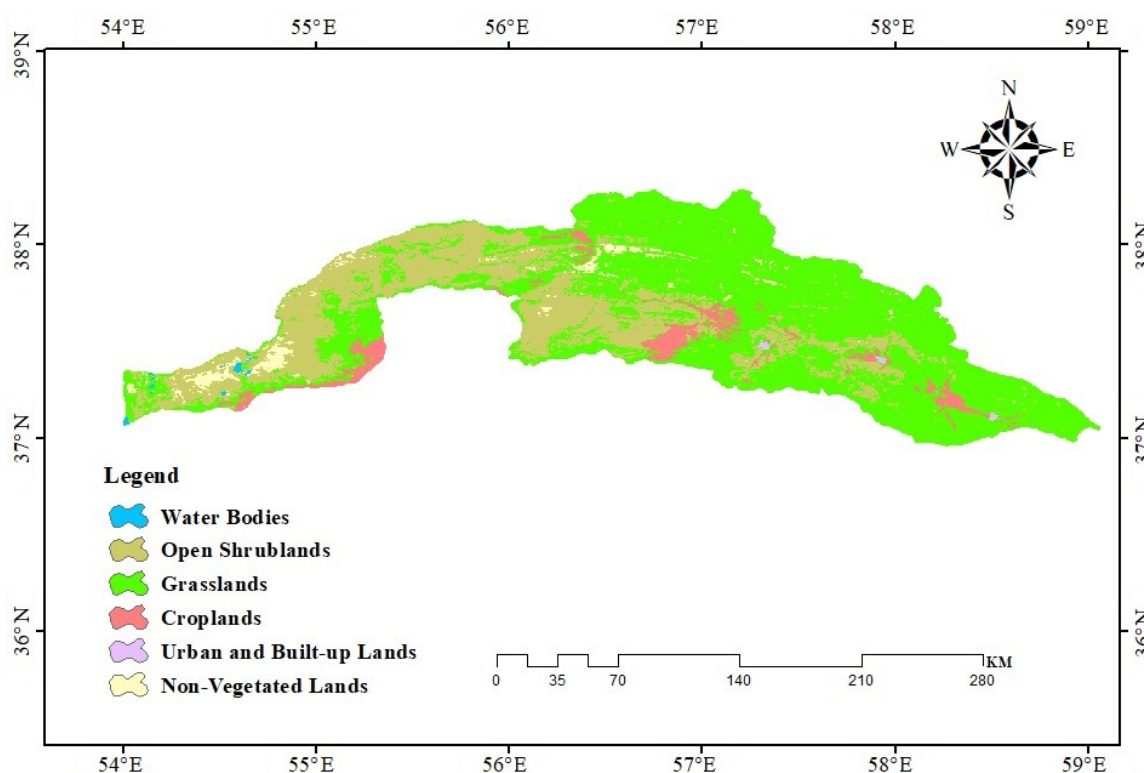


Figure 2. Land cover map of Atrak basin (map for 2020).

2.2. Data

This study utilized the 16-day 250 m Enhanced Vegetation Index (EVI) data from MOD13Q1, 8-day 1 km Land Surface Temperature (LST) data from MOD11A2, and monthly precipitation data obtained from the CHIRPS satellite to investigate vegetation dynamics and its correlation with rainfall patterns spanning the timeframe of 2003 to 2021 (Table 1). The initial step involved calculating seasonal and yearly average vegetation cover, land surface temperature, and precipitation values using the ArcGIS program. The winter, spring, and summer vegetation indices were derived from averages of six images each, while autumn vegetation was computed from averages of five images. Additionally, annual coverage was computed from averages of twenty-three images. Furthermore, a total of 828 daily images for the land surface temperature were downloaded for the study area, with

46 images per year. These image datasets were sourced from the United States Geological Survey website (www.usgs.gov (accessed on 10 July 2023)). To ascertain the trend of spatial alterations in vegetation and to detect anomalies for assessing vegetation shifts within the second decade of the analyzed time series (2011 to 2021) relative to the average reference period (2003 to 2011), the study utilized the Google Earth Engine system. Furthermore, based on each year's land cover map, croplands were distinguished from other land classes in land cover maps and analyzed on annual EVI satellite images.

Table 1. The datasets and satellite images used in the study.

Data	Source	Characteristics
EVI	MODIS (MOD13Q1)	16-day composite EVI, 250 × 250 m
LST	MODIS (MOD11A2)	8-day composite LST, 1 × 1 km
Precipitation	CHIRPS	Monthly CHIRPS precipitation, 0.05° × 0.05°

Rainfall data for the winter season were computed from an average of three images spanning December to February; for the spring season, they were derived from an average of three images from March to May; the summer season's data relied on an average of three images for June to August; the autumn season's information was obtained from an average of three images between September and November. Furthermore, annual rainfall statistics were generated from an average of twelve images, spanning January to December. After generating seasonal and yearly image datasets, all pixel values corresponding to vegetation cover and precipitation were compiled into Excel spreadsheets. These data were then subjected to a comprehensive analysis involving classification, graphical representation, quantification of precipitation and vegetation shifts, calculation of both seasonal and annual Standardized Precipitation Index (SPI) values, and coverage area estimation.

MODIS Data

MODIS stands as a pivotal and practical satellite within the domain of monitoring alterations across the Earth's surface, oceans, and atmosphere. Its dataset and an array of diverse products have been accessible since 2000 and are integrated into two satellite platforms, Terra and Aqua. Among its noteworthy capabilities, it boasts a high radiometric resolution of 12 bits and encompasses 36 spectral bands spanning from 0.4 to 14.4 μm. It exhibits variable resolutions ranging from 250 m to 1000 m, tailored to specific spectral bands. The satellite also offers a time resolution of 1 to 2 days, a facet that has positioned it as one of the most extensively utilized platforms in the realm of environmental investigations. From the MODIS images, the Enhanced Vegetation Index (EVI) and land surface temperature (LST) were obtained directly.

2.3. Methods

2.3.1. Enhanced Vegetation Index (EVI)

A notable advantage of the EVI index is its ability to mitigate atmospheric and aerosol-related influences [40]. The EVI indices were directly downloaded and subsequent relationships were employed to compute the EVI averages for both the annual and seasonal assessments:

$$\text{Winter vegetation} = \frac{\sum(\text{image 353 to image 65})}{6} \quad (1)$$

$$\text{Spring vegetation} = \frac{\sum(\text{image 81 to image 161})}{6} \quad (2)$$

$$\text{Summer vegetation} = \frac{\sum(\text{image 177 to image 257})}{6} \quad (3)$$

$$\text{Fall vegetation} = \frac{\sum(\text{image 273 to image 337})}{5} \quad (4)$$

$$\text{Annual vegetation} = \frac{\sum(\text{image 17 to image 1})}{23} \quad (5)$$

2.3.2. Land Surface Temperature (LST)

The Earth's surface temperature is a critical parameter in environmental studies and assessments, such as monitoring drought conditions. Each pixel represents the temperature of the Earth's surface, reflecting the heat emitted by various objects. Therefore, in remote sensing, the surface temperature of the Earth for each pixel corresponds to the average temperature of the different types of surface cover [41]. Annual and seasonal averages of these images were calculated as:

$$\text{Winter LST} = \frac{\sum_{i=1}^{12} \text{LST}_i}{12} \quad (6)$$

$$\text{Spring LST} = \frac{\sum_{i=13}^{24} \text{LST}_i}{12} \quad (7)$$

$$\text{Summer LST} = \frac{\sum_{i=25}^{36} \text{LST}_i}{12} \quad (8)$$

$$\text{Fall LST} = \frac{\sum_{i=37}^{46} \text{LST}_i}{12} \quad (9)$$

$$\text{Yearly LST} = \frac{\sum_{i=1}^{46} \text{LST}_i}{46} \quad (10)$$

where the index (i) counts the images of each year in date order.

2.3.3. Standardized Precipitation Index (SPI)

The standard precipitation index (SPI) is an index often used for assessing drought conditions. Calculation of SPI for each specific region is based on long-term rainfall statistics, which are usually fitted to a probability distribution function (gamma probability function). The resulting function can be used to find the cumulative probability of rainfall for a station and for a specific month and time scale. In practice, the following fact is often utilized: for a random variable X with a gamma distribution, the variable $Z = \sqrt[3]{X}$ has an approximately normal distribution. Using this fact, the following approximate method for calculating the SPI coefficient can be proposed:

$$\text{For a given value } x \geq 0 \text{ SPI} = \frac{\sqrt[3]{x_i} - \hat{\mu}}{\text{SD}} \quad (11)$$

where $\hat{\mu}$ is the average and SD is the standard deviation for data subjected to the transformation $x_i \rightarrow \sqrt[3]{x_i}$. The stages leading to the determination of the SPI indicator are the normalization of periodic precipitation sums using $x_i \rightarrow \sqrt[3]{x_i}$, verification of the hypothesis regarding the compatibility of the distribution of the transformed variable with the normal distribution using the Shapiro–Wilk test, and the standardization of transformed data and determination of the SPI.

SPI relies on quantifying the divergence of rainfall values from their long-term average over a designated period, rendering it a preferable option compared to other meteorological drought indices [42]. The classes associated with this index are displayed in Table 2.

Table 2. Classification of drought severity based on SPI.

Index Values	Class
More than 2	Extremely wet
1.5 to 1.99	Very wet
1 to 1.49	Moderate wet
−0.99 to 0.99	Near Normal
−1 to −1.49	Moderate dry
−1.49 to −1.99	Severely dry
−2 and less	Extremely dry

2.3.4. Vegetation Condition Index (VCI)

The Vegetation Condition Index (VCI) was introduced in 1995 [43]. This index reflects the vegetation status within a specific area, calculated based on the minimum and maximum Normalized Difference Vegetation Index (NDVI) values spanning several years. The VCI is expressed as a percentage. Since the Enhanced Vegetation Index (EVI) is an advancement of the NDVI, the EVI was utilized for calculating the VCI index. The numerical range of the VCI varies between 0 and 100. Values approaching zero signify stress and severe drought within the region, while values approaching 100 indicate favorable vegetation conditions and amelioration of drought conditions [44]. It is calculated as:

$$VCI = \left(\frac{EVI - EVI_{min}}{EVI_{max} - EVI_{min}} \right) \times 100 \tag{12}$$

In the above relationship, EVI is the improved seasonal or annual vegetation cover index, while EVI_{min} and EVI_{max} are the minimum and maximum long-term EVI in the entire study area in the assessed period (in the case of this paper it was 2003–2021).

2.3.5. Anomaly calculation

The standardized anomaly, also known as the Z-score, quantifies the extent of deviations from the mean of the quantity being analyzed. It is calculated using the formula [45]:

$$Z_{ij} = \frac{X_{ij} - U}{\sigma_{ij}} \tag{13}$$

Here, i represents the assessed period, j stands for the time scale, X_{ij} is an analyzed parameter in a given year, U represents the mean value for the analyzed period, and σ_{ij} indicates the standard deviation. Positive values of the standardized anomaly indicate that the values being assessed are larger than the mean, while negative values indicate that the values are smaller than the mean. Values greater than $|2|$ indicate that the result is abnormal [46].

2.3.6. Pearson Correlation

The correlation coefficients were calculated using Pearson correlation, which measures the strength of the linear relationship between two variables, one dependent and the other independent [47]. It ranges in value from -1 to 1 , with -1 meaning a total negative linear correlation, 0 meaning that two quantities are not correlated, and $+1$ meaning a total positive correlation. The Pearson correlation, being the first formal measure of correlation, remains one of the most widely used measures for assessing relationships between variables [48]:

$$R_{xy} = \frac{\sum(x_i - \bar{X}) \sum(y_i - \bar{y})}{\sqrt{\sum(x_i - \bar{X})^2} \sqrt{\sum(y_i - \bar{y})^2}} \tag{14}$$

where \bar{x} denotes the mean of x and \bar{y} denotes the mean of y . The significance of the correlation coefficients was judged using a t -test. The trends were fitted to the data using linear regression.

3. Results

According to Figure 3, which depicts the average vegetation cover spanning 19 years for each EVI date, it is evident that the more rapid phase of vegetation growth commences in January during the winter season and reaches its zenith in April, registering at 39.5% (equivalent to 10,434.11 km²). Thus, the spring period from March to June exhibits the most extensive vegetation coverage. Starting from the initial days of May, the vegetation gradually diminishes, culminating in the lowest extent of vegetation around November at 1.16% (amounting to 307.3224 km²), characterizing the late autumn period. Notably, a slight increase of 2.5% in vegetation occurred between the end of December and the beginning of January. Between June and September, corresponding to the summer season, the dehydration of plants contributes to a decrease in the vegetation area. Additionally, due to the positive correlation between the evaporation of water from leaf surfaces and the ground, the available water for plants in the soil increases, simultaneously reducing the plants' daily water requirements Początek formularza [27].

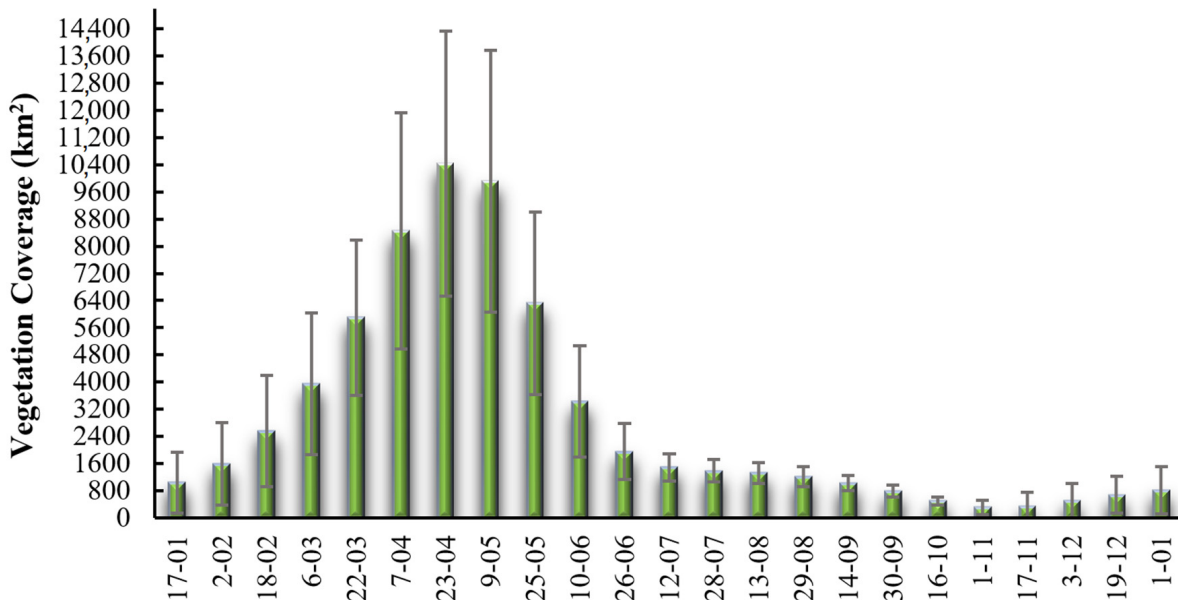


Figure 3. Nineteen-year averages of the Atrak’s basin vegetation coverage during the assessed period (2003–2021) for specific dates for which the EVI images were available, with the standard deviations (SD) marked by grey whiskers.

Based on Figure 4, it is evident that during this specific season, the distribution of vegetation cover presents a notable contrast between the eastern half of the basin situated in North Khorasan province and the western half located in Golestan province. This discrepancy is attributed to the region’s temperate and mountainous climate. During the summer season, urban areas predominantly host green trees and parks. Furthermore, elevated regions experience lower temperatures, which subsequently decrease evaporation and transpiration rates in plants, effectively sustaining vegetation in the research area. Consequently, in this particular season, vegetation is more prevalent in the eastern half of the basin within North Khorasan province, characterized by a moderate mountainous climate, compared to the western half encompassing a portion of Golestan province.

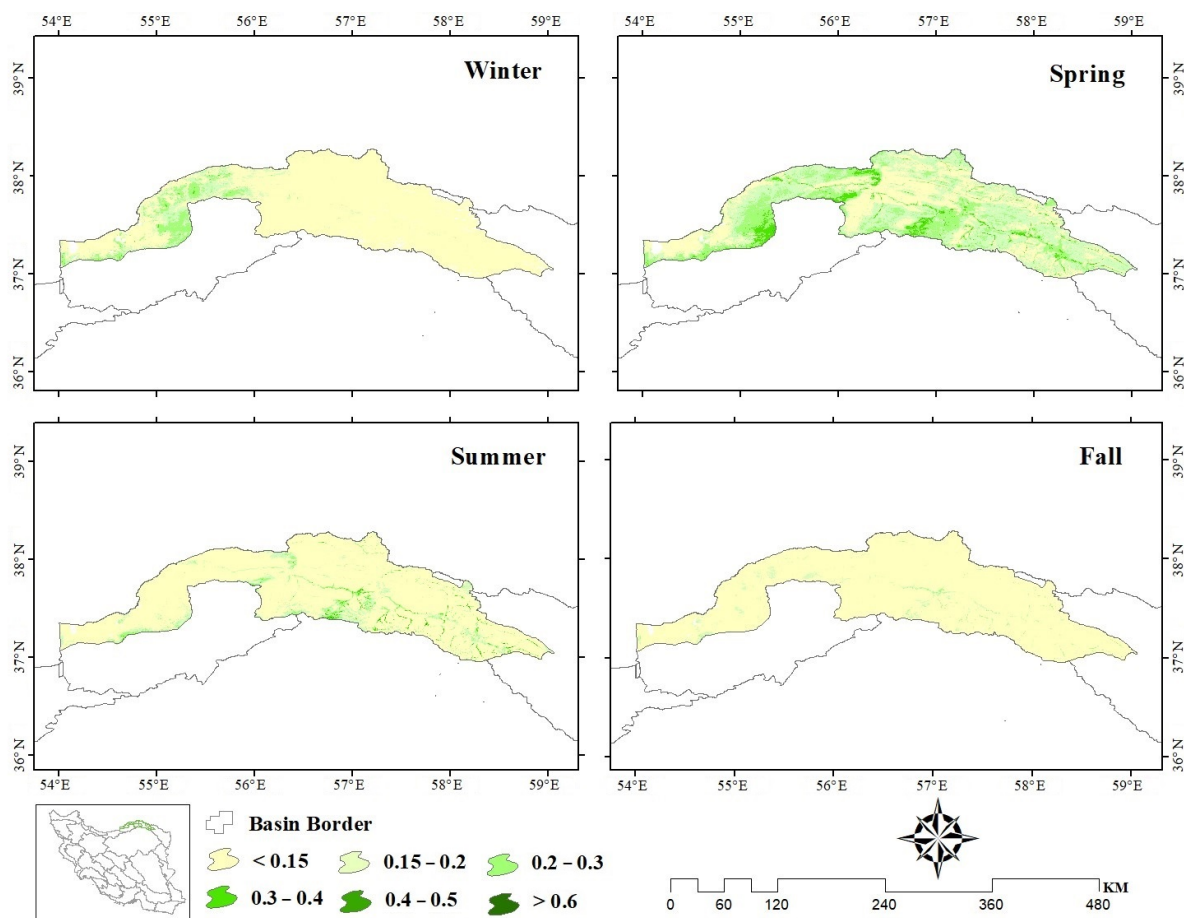


Figure 4. Seasonal average EVI values in the Atrak basin area during 2003–2021.

At the end of September, coinciding with the onset of autumn, only urban locales retain their verdant state, as water evaporation from tree leaves becomes full. In the heart of the winter season, spanning 17 January to 18 February, substantial changes in vegetation become evident due to intermittent rains and slight temperature fluctuations. Notably, the distribution of vegetation in the western half of the basin within Golestan province, which receives the most winter rainfall, becomes conspicuously distinct.

Based on Figure 5, which depicts the seasonal shifts in vegetation cover throughout the analyzed time series, the spring season consistently exhibits the highest vegetation coverage. Specifically, in the years 2010, 2016, and 2019, the peak was observed at 45.28% (equivalent to 11,966.7 km²), 43.45% (equivalent to 11,483.4 km²), and 54.50% (equivalent to 14,404.18 km²), respectively.

As shown in Figure 6, detailing the trend of variations during the second decade (2011–2021) in comparison to the average of the first decade (2003–2010) within the studied time series, a discernible pattern emerges. The eastern sectors of the basin, located within North Khorasan province and a segment of Razavi Khorasan, contrast with the western areas comprising the northern portion of Golestan province. The former regions exhibit an increasing trend, while the central and western sections of the basin have witnessed varying degrees of decline, with certain parts displaying no significant change.

The findings reveal that over the examined statistical timeframe, the years 2008, 2014, 2017, and 2021 exhibited the lowest total vegetation coverage, accounting for 4.89%, 5.75%, 6.81%, and 6.61% respectively, of the entire Atrak basin area (as shown in Table 3). Conversely, during the years of abnormally high precipitation sums, such as 2004 (396.7 mm), 2007 (400.4 mm), 2009 (386.8 mm), and 2019 (429.7 mm), the corresponding vegetation cover percentages were 12.8%, 10.78%, 9.6%, and 18.25%, respectively (Figure 7).

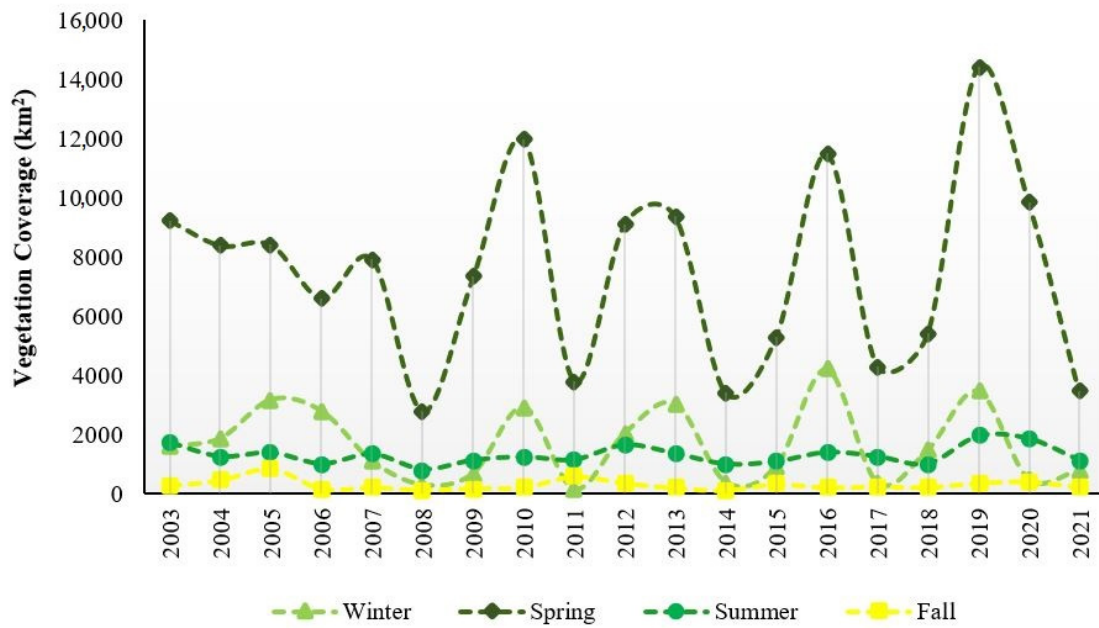


Figure 5. Seasonal changes in VC values in the period from 2003 to 2021.

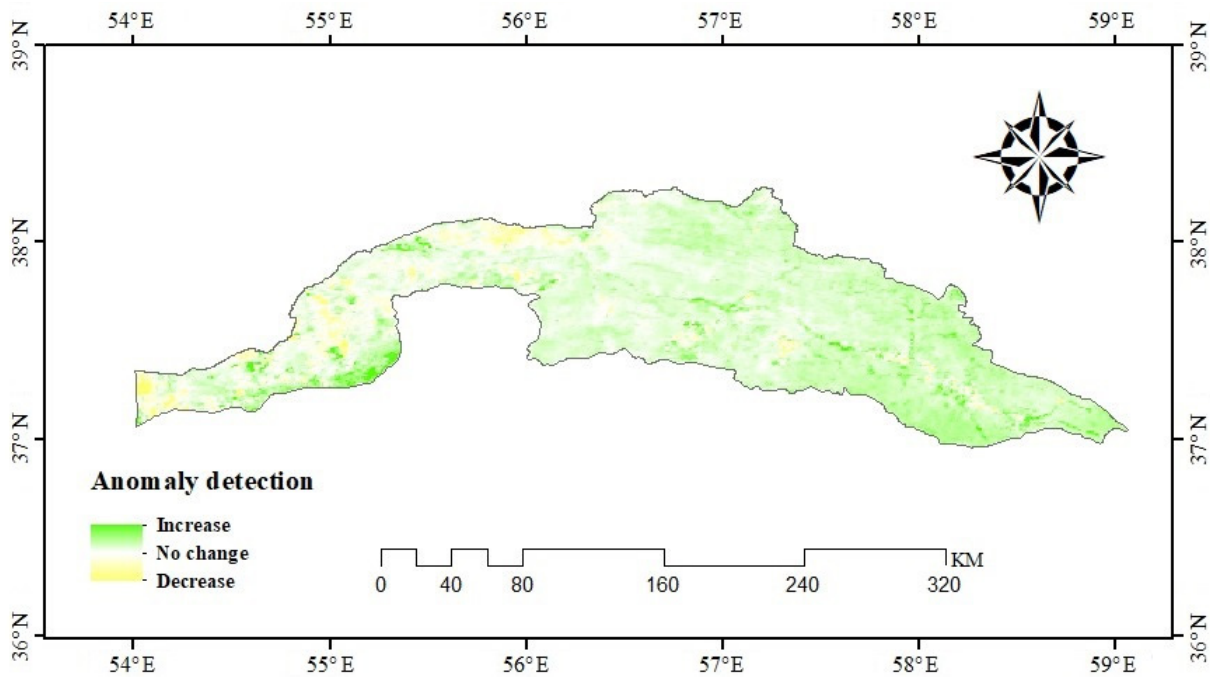


Figure 6. The values of slopes of trend lines fitted into the EVI 2003–2021 anomaly plots for each pixel showing whether abnormal EVI increases (green) or decreases (yellow) were observed.

Examining vegetation classes, the VC area classified as poor vegetation (EVI 0.2–0.3) was 998 km² in 2008, reaching its peak of 3135 km² in 2019. The moderate coverage class had the largest expanse in 2019, and it was 1090 km², while the lowest occurred in 2008 with 215 km². Across the categories of good, dense, and very dense cover, the most substantial areas observed in 2019 were 402, 147, and 50 km², respectively. Conversely, the smallest extents were recorded in 2008, with 60, 16, and 4 km², respectively. Overall, the 19-year average areas for poor, moderate, good, dense, and very dense cover were 1979, 587, 205, 70, and 24 km², respectively, encompassing the entire basin area.

Table 3. The area of coverage of different EVI floors in the study area in terms of (km²) during the period from 2003 to 2021.

Year	EVI 0.2–0.3	EVI 0.3–0.4	EVI 0.4–0.5	EVI 0.5–0.6	EVI > 0.6	Total Area (km ²)	Total Area (Percent)
2003	2349	727	258	84	28	3447.11	13.04
2004	2281	644	194	58	18	3193.24	12.08
2005	2263	767	264	87	30	3409.14	12.90
2006	2069	604	175	60	17	2923.80	11.06
2007	1912	578	234	92	33	2849.24	10.78
2008	998	215	60	16	4	1293.10	4.89
2009	1711	523	196	72	38	2540.67	9.61
2010	2518	915	341	118	39	3931.59	14.88
2011	1451	313	90	25	5	1884.73	7.13
2012	2435	725	253	78	22	3511.78	13.29
2013	2476	753	248	84	33	3593.63	13.60
2014	1155	263	76	20	5	1519.33	5.75
2015	1645	399	134	40	12	2229.28	8.43
2016	2688	974	382	141	65	4250.14	16.08
2017	1314	326	116	35	8	1799.74	6.81
2018	1525	408	153	63	26	2175.28	8.23
2019	3135	1090	402	147	50	4824.68	18.25
2020	2337	625	229	83	28	3302.07	12.49
2021	1335	296	86	23	5	1746.18	6.61
Average	1979	587	205	70	24	2864	11

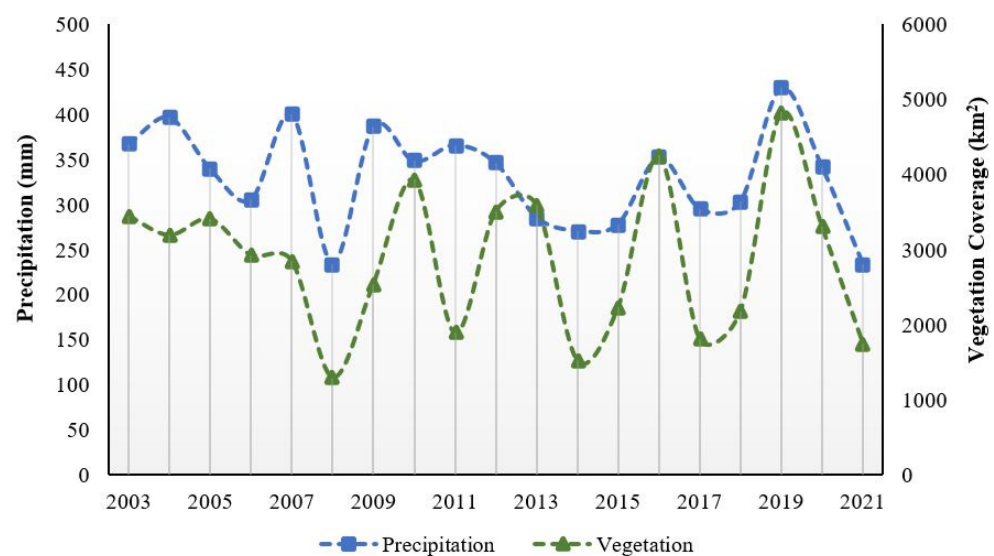


Figure 7. Annual changes in precipitation and vegetation during the period from 2003 to 2021.

Figure 8 illustrates the correlation between annual vegetation cover and the severity of drought, employing the EVI and VCI indices, within the Atrak basin throughout the study duration from 2003 to 2021. Using the classification established in the scientific literature [43], regions experiencing drought conditions and those not affected by drought are classified based on VCI index values ranging between 0% and 35%, and between 35%

and 100%, respectively. Across the entire basin, which spans approximately 26,430 km², the vegetation area displays annual fluctuations, ultimately yielding an average vegetation coverage of 2864 km² (11% of the total study area) over the entire period. The VCI index shows that the most pronounced instances of drought were in the years 2008, 2011, 2014, 2017, and 2021, registering percentages of 95.93%, 71.5%, 67.8%, 61.5%, and 57.6% of the total area, respectively. Conversely, the least pronounced droughts were in 2010, 2013, 2016, 2019, and 2020, encompassing 2.6%, 5.4%, 2%, 2.19%, and 9.7% of the total area, respectively.

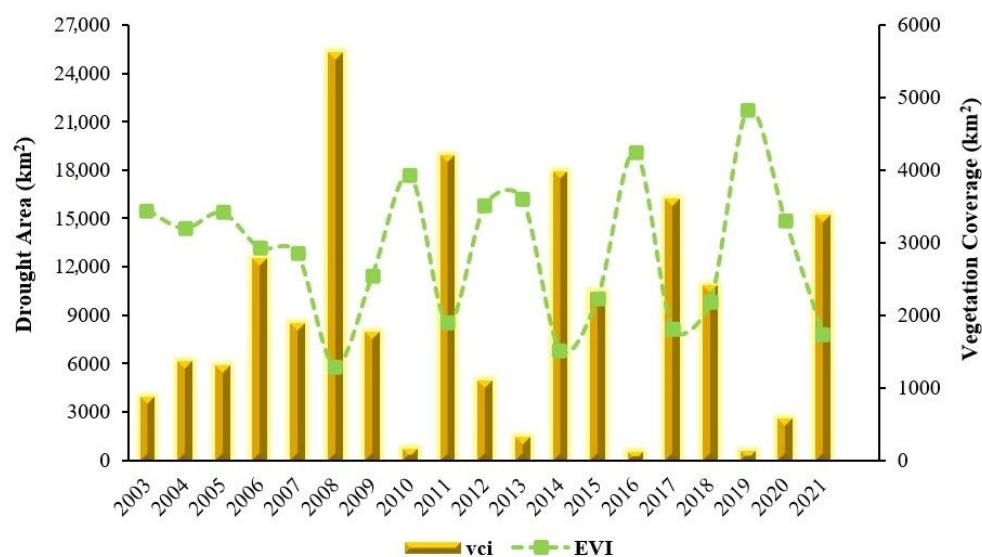


Figure 8. Changes in the EVI vegetation area and drought area of the Atrak basin during the period from 2003 to 2021.

Figure 9 presents a visualization of vegetation density during both wet and dry years. From this representation, it becomes apparent that 2008 stands out as the driest year, characterized by a VCI index of 95.9%, whereas 2016 emerges as the wettest year, marked by a VCI index of 1.98%, within the scope of the analyzed time series. Additionally, during years with higher precipitation, the western regions of the basin, situated in Golestan province, exhibit greater vegetation density compared to the eastern and central parts of the basin in North Khorasan and Razavi provinces. This discrepancy is primarily attributed to the substantial average annual rainfall experienced in these areas. Notably, certain locales might demonstrate disparities in rainfall patterns, either high or low, due to influencing environmental factors like topography.

Across the examined time series, the years 2004, 2007, 2009, and 2019 stand out as having the highest average rainfall, with 396.7 mm, 400 mm, 386.8 mm, and 429.7 mm respectively. These values indicate conditions ranging from a moderate wet year to a very heavy wet year. Conversely, the years 2008, 2014, and 2021 exhibit the lowest annual rainfall averages of 234 mm, 270.7 mm, and 233.6 mm respectively, characterizing conditions of moderate and severe drought. The remaining years fall within the range of normal conditions. Furthermore, the years 2010, 2016, and 2019 notably display the most extensive vegetation coverage, spanning areas of 3931.5, 4250.1, and 4824.6 km², respectively. In contrast, the years 2008, 2014, and 2021 exhibit the smallest vegetation coverage areas, corresponding to 129, 1519.3, and 1746.1 km², respectively. Additionally, the highest average temperature was recorded in 2021, with a temperature of 28.2 °C, and in 2017 and 2018, with temperatures of 27.6 and 27.4 °C, respectively, and the year 2003 has the lowest average temperature at 24 °C (Figure 10). Within the winter season, particularly noteworthy are the years 2010 and 2019, characterized by the highest recorded rainfall levels of 158 mm and 156 mm, respectively. These values signify extremely wet conditions, as confirmed by SPI results. Furthermore, the years 2014 and 2021 recorded the lowest rainfall at 86.5 mm

and 82.3 mm, indicating a state of severe drought. On the other hand, the largest vegetation coverage was observed in 2016, spanning an area of 4190 km², while the smallest vegetation area occurred in 2011, covering an area of 122.6 km². The highest average LST was in 2018, with a temperature of 11.7 °C, while the lowest average temperature was recorded in 2008 and 2012, with 5.21 and 5.12 °C, respectively.

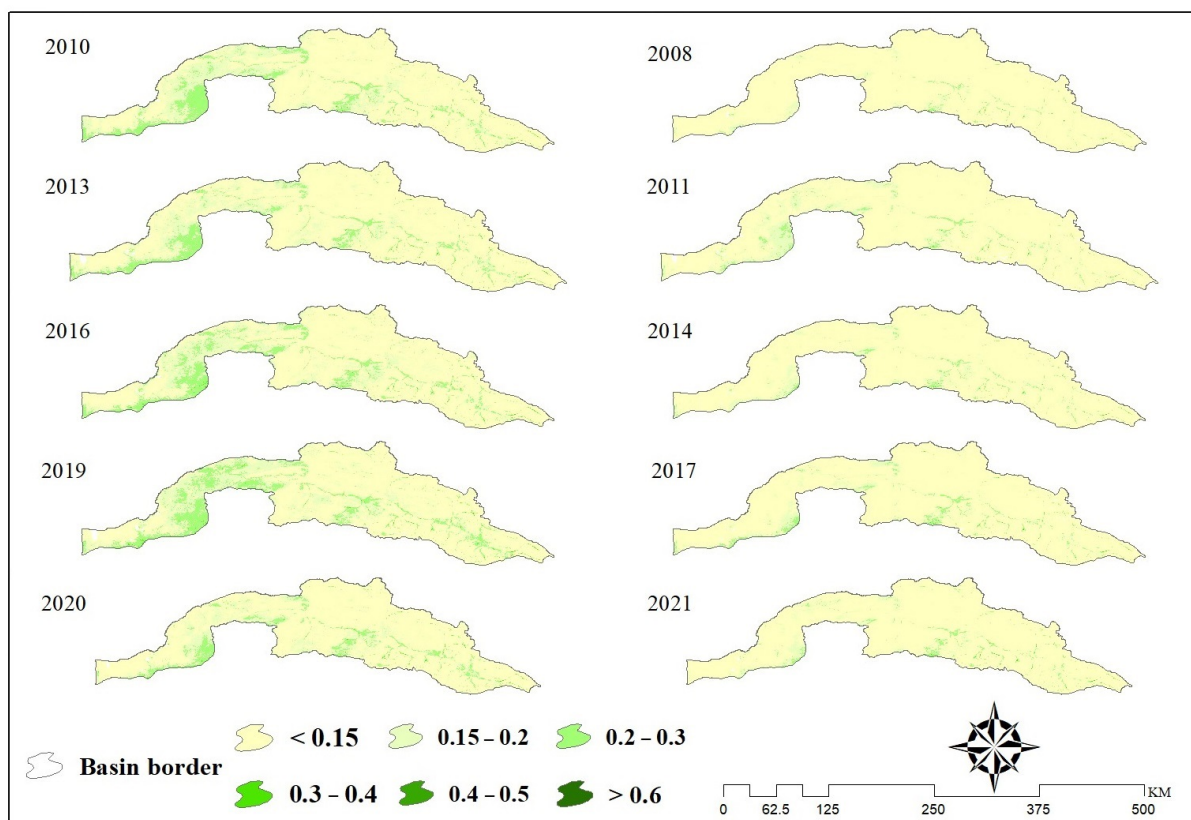


Figure 9. The EVI values in selected dry and wet years in the Atrak basin during the assessed period from 2003 to 2021.

Transitioning to the spring season, the highest recorded rainfall of 227.5 mm was documented in 2019, signaling a classification as an extremely wet year according to SPI results. Conversely, 2015 experienced notably low rainfall at 78.2 mm, indicative of a state of severe drought. Within this season, the maximum vegetation coverage occurred in 2019, encompassing an area of 14,404 km², while the minimum was recorded in 2008 at 2776.6 km². The highest average temperature, 33.34 °C, was recorded in 2021, and the lowest average temperature was recorded in 2003 with a temperature of 25.7 °C. Moving to the summer season, the peak rainfall of 31.7 mm transpired in 2004, signifying an extremely wet year, while 2021 had the lowest rainfall at 15.7 mm, reflecting a moderate state as per the SPI. Notably, the highest vegetation extent was documented in 2019, covering an area of 1929.8 km², while the smallest occurred in 2008 at 799.1 km². Additionally, the years 2017 and 2021 had the highest average temperatures, of 43.6 and 43 °C, respectively, while in the years 2003 and 2009 the lowest average temperatures were recorded for this season, with temperatures of 38.8 and 39 °C, respectively. Within the autumn season, the years 2011 and 2018 experienced the highest recorded rainfall at 76 mm and 62.7 mm, respectively, aligning with an extreme wet and very wet year classification based on SPI results. In contrast, the lowest autumnal rainfall was observed in 2021, measuring 28.2 mm and corresponding to severe drought. Correspondingly, the maximum vegetation coverage materialized in 2005, spanning an area of 820.9 km², while the minimum was noted in 2014 at 102.4 km². The highest LST for this season was in 2010, with a temperature of 24.8 °C, and the lowest was in 2011, with a temperature of 19 °C (Figure 10).

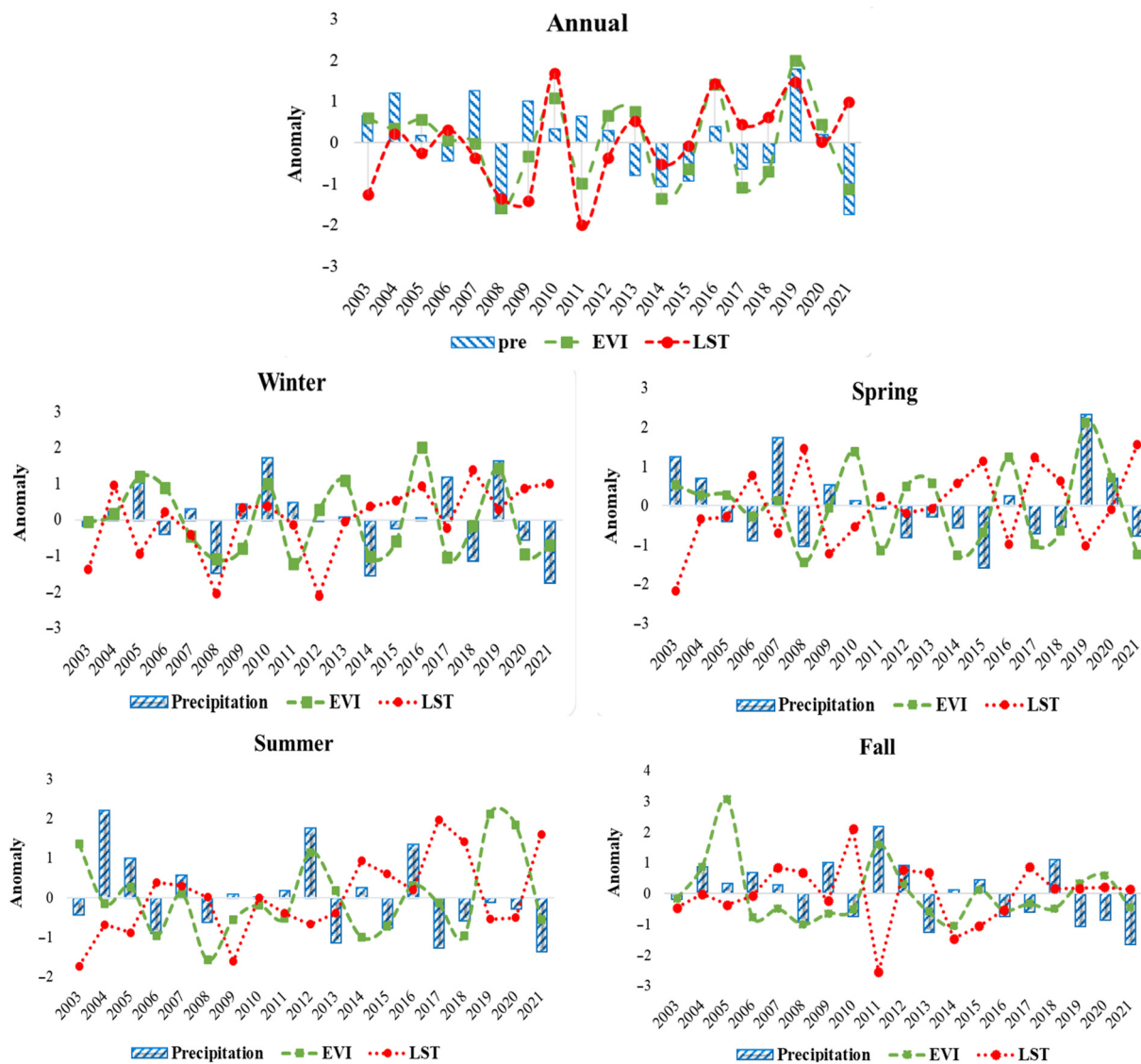


Figure 10. Time series of precipitation, LST, and EVI annual and seasonal changes in the Atrak basin from 2003 to 2021.

While rainfall is commonly perceived as the primary driver of vegetation changes, it is noteworthy that years with elevated rainfall levels do not necessarily correspond to significant shifts in vegetation patterns. Therefore, other influential environmental factors such as topography, soil composition, and salinity must also be considered in this context [49]. According to Table 4, a significant relationship was observed between annual vegetation cover and temperature in spring ($-0.520, p = 0.01$) and summer ($-0.345, p = 0.05$). Additionally, a significant relationship ($-0.380, p = 0.05$) exists between annual temperature and summer vegetation. Conversely, significant negative relationships were noted between spring temperature and winter, as well as between spring and summer vegetation. Moreover, summer temperature exhibits a significant negative correlation with spring and summer vegetation. Generally, when humidity is low, particularly during the summer season when water availability limits plant growth, a negative correlation between temperature and vegetation is typical [50].

Table 4. Correlation between LST and EVI during the assessed period from 2003 to 2021.

LST	EVI Winter	EVI Spring	EVI Summer	EVI Fall	EVI Annual
Winter	0.053	0.006	−0.193	−0.018	−0.041
Spring	−0.357 *	−0.520 **	−0.415 *	−0.099	−0.520 **
Summer	−0.205	−0.345 *	−0.357 *	−0.228	−0.345 *
Fall	0.041	0.135	0.076	−0.099	0.111
Annual	−0.111	−0.298	−0.380 *	−0.228	−0.322

* Denotes a significant correlation at $p = 0.05$ ** Denotes a significant correlation at $p = 0.01$.

Table 5 presents the outcomes of the correlation analysis examining the relationship between rainfall and vegetation, considering both seasonal and annual perspectives over 19 years. The analysis revealed several noteworthy findings. Specifically, a substantial correlation exists between spring precipitation and the Enhanced Vegetation Index (EVI) during both spring and summer (0.439, 0.450, $p = 0.01$), and a statistically significant association is observed between annual precipitation and EVI during the spring and summer seasons (0.462, $p = 0.01$) and (0.404, $p = 0.05$), respectively. Additionally, there is a significant correlation between winter rainfall and annual EVI (0.333, $p = 0.05$). Notably, no significant correlation is observed between precipitation and annual and seasonal EVI in the autumn season. Furthermore, a statistically significant correlation is identified between spring precipitation and the annual EVI, once again (0.392, $p = 0.05$). This finding underscores the highest level of correlation between spring precipitation and EVI-related vegetation trends. To gain a deeper understanding of the annual and seasonal changes in EVI during the period of the study, Table 6 presents the percentage of seasonal and annual changes in vegetation cover, and Figure 11 illustrates the distribution of annual vegetation (in percent) compared to annual and seasonal precipitation in the study area.

Table 5. Correlation between precipitation and EVI during the assessed period from 2003 to 2021.

Precipitation	EVI Winter	EVI Spring	EVI Summer	EVI Fall	EVI Annual
Winter	0.240	0.310	0.251	0.263	0.333 *
Spring	0.181	0.439 **	0.450 **	0.158	0.392 *
Summer	0.170	0.240	0.205	0.193	0.240
Fall	−0.111	−0.205	−0.193	−0.170	−0.158
Annual	0.251	0.462 **	0.404 *	0.228	0.439 **

* Denotes a significant correlation at $p = 0.05$ ** Denotes a significant correlation at $p = 0.01$.

Considering the crucial role of agricultural lands in the country's food security, economy, and the preservation of biodiversity [51], as well as their relationship with climate change [52,53], the changes occurring in the agricultural land class in the Atrak basin area was investigated separately from other land classes. According to Table 7, the years 2003, 2007, and 2020, with an area of 751 km², followed by 2004 with 756 km² and 2019 with 758 km², had the highest area of croplands. In contrast, 2008 with an area of 525 km², 2011 and 2014 with 573 km², 2015 with 588 km², and 2021 with an area of 486 km² had the lowest cropland area. The largest area of cropland in this basin falls into the "very poor" and "poor" classes, covering 393 and 269 km², respectively. According to Figure 12 and Table 8, a significant decreasing trend can be observed in the "very poor" and "dense" classes (−0.392, −0.415, $p = 0.05$), while the "moderate" class shows a significant increasing trend (−0.551, $p = 0.01$). However, a significant trend of changes is not observed in the "poor" classes and the total annual cropland area.

Table 6. Changes in the percentage of the total vegetation area for yearly and seasonal data in the Atrak basin (2003–2021).

Year	Annual	Winter	Spring	Summer	Fall
2003	13.04	5.95	34.85	6.42	0.97
2004	12.08	7.02	31.69	4.67	1.66
2005	12.90	11.98	31.78	5.18	3.11
2006	11.06	10.48	24.95	3.73	0.57
2007	10.78	4.06	29.95	4.97	0.75
2008	4.89	1.03	10.51	3.02	0.42
2009	9.61	2.48	27.65	4.20	0.65
2010	14.88	10.98	45.28	4.63	0.74
2011	7.13	0.46	14.39	4.24	2.13
2012	13.29	7.64	34.43	6.18	1.27
2013	13.60	11.41	35.39	5.06	0.68
2014	5.75	1.36	12.86	3.70	0.39
2015	8.43	3.37	19.97	4.02	1.15
2016	16.08	15.85	43.45	5.20	0.72
2017	6.81	4.69	16.27	4.69	0.86
2018	8.23	5.46	20.43	3.73	0.76
2019	18.25	13.03	54.50	7.30	1.29
2020	12.49	1.76	37.21	7.00	1.47
2021	6.61	2.84	13.00	4.20	0.78

Table 7. The coverage area for different cropland EVI classifications in the study area (km²) during the period from 2003 to 2021.

Year	EVI 0.1–0.2	EVI 0.2–0.3	EVI 0.3–0.4	EVI > 0.4	Total Area (km ²)
2003	461.75	287.19	1.69	0.38	751
2004	489.75	261.94	4.25	0.19	756.13
2005	433.31	300.63	5.44	0.25	739.63
2006	502.06	213.63	2.25	0.13	718.06
2007	432	316	3.56	0.13	751.75
2008	467.75	55.25	2.63	0	525.69
2009	339.25	282.25	4.81	0.25	626.56
2010	301.19	391.5	8.19	0.31	701.19
2011	468.94	102.44	2.38	0.13	573.88
2012	360.44	265.81	4.94	0.25	631.44
2013	322.88	408.56	5.06	0.19	736.69
2014	466.44	103.38	3.75	0.06	573.63
2015	356.63	225.69	6	0.19	588.50
2016	279.13	442.06	13.94	0.31	735.44
2017	465.44	182.44	6.13	0.13	654.13
2018	338.63	296.44	5.06	0.06	640.19
2019	277.13	464.63	16.88	0	758.63
2020	347.31	391.75	12.75	0.06	751.88
2021	357.19	121.75	7.31	0.06	486.31
Average	393	269.13	6.16	0.16	668.46

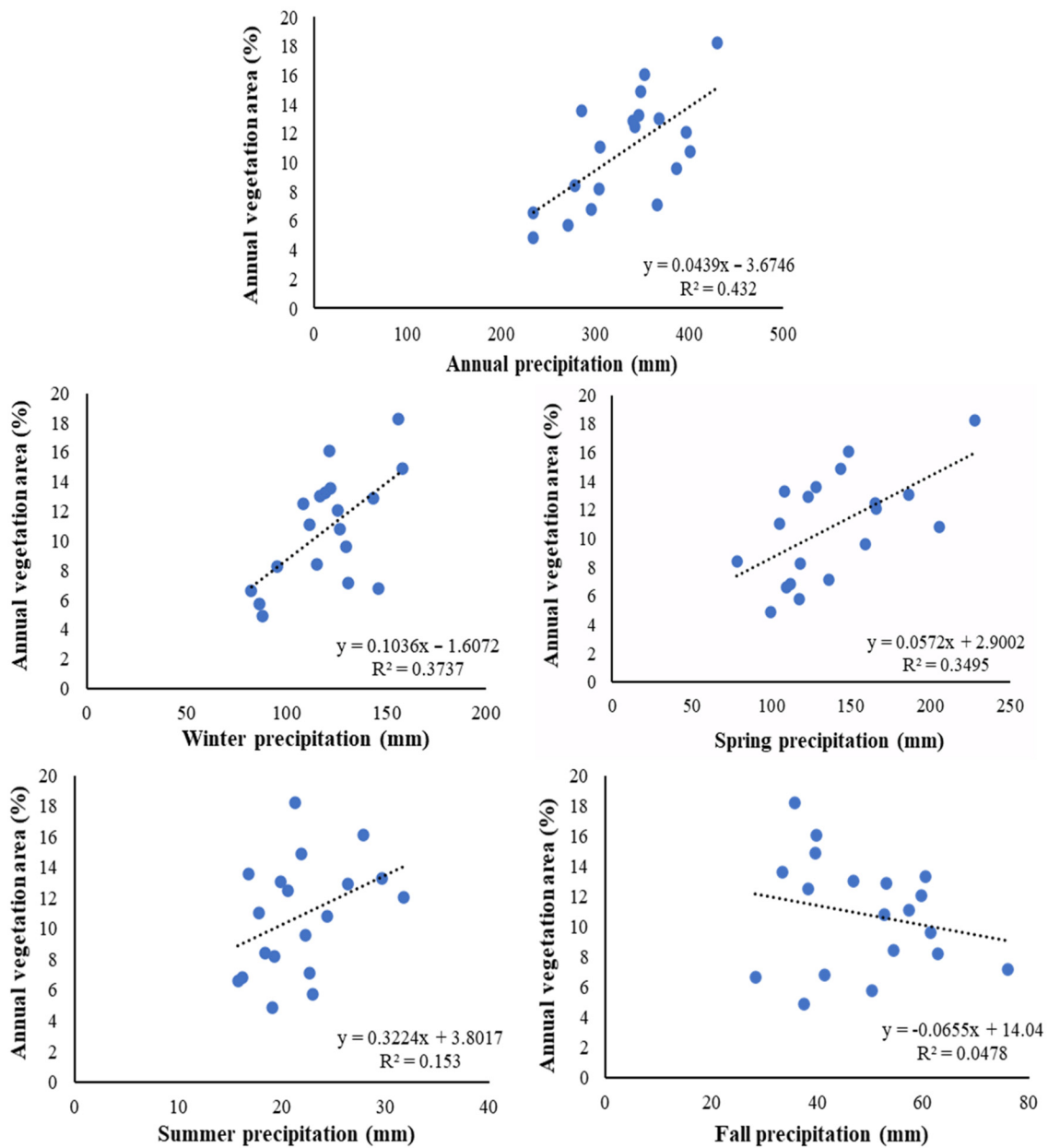


Figure 11. Distribution (scatter plot) of annual vegetation cover (in percent) dependence on the annual and seasonal rainfall in Atrak Basin during the period of 2003–2021. Data is represented by blue dots, while the dotted line indicates the linear fit.

Table 8. The linear trend coefficients for different classes of cropland during 2003–2021.

	EVI 0.1–0.2	EVI 0.2–0.3	EVI 0.3–0.4	EVI > 0.4	Total Area (km ²)
Year	−0.392 *	0.123	0.551 **	−0.415 *	−0.158

* Denotes a significant trend at $p = 0.05$. ** Denotes a significant trend at $p = 0.01$.

According to Table 9, which presents the correlation between the total area of croplands in the Atrak Basin and annual and seasonal rainfall, a significant relationship between the total area of cropland and winter and spring rainfall can be observed (0.333, $p = 0.05$ and 0.556, $p = 0.01$, respectively). Additionally, concerning annual precipitation, a very strong and significant trend is evident (0.532, $p = 0.01$). As shown in Figure 13, during the winter

and summer seasons, as well as annually, a positive relationship between precipitation and cropland is observed (an increase in rainfall is followed by an increase in crop cover).

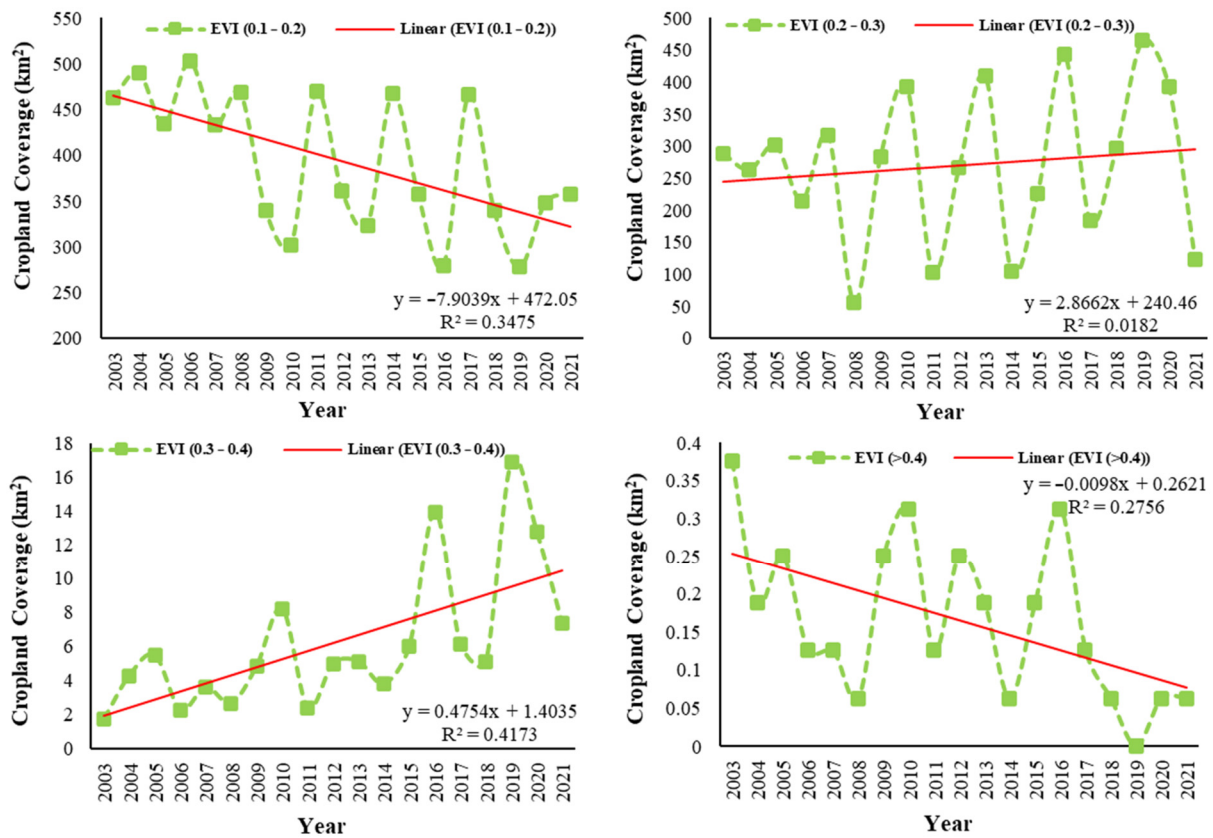


Figure 12. EVI trend of cropland land class during 2003–2021.

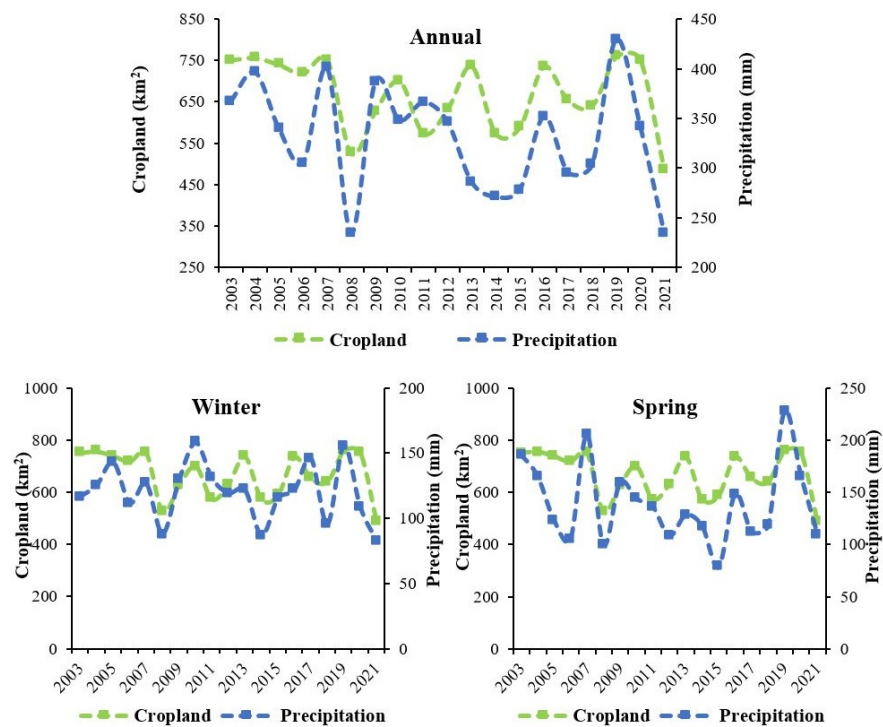


Figure 13. Cont.

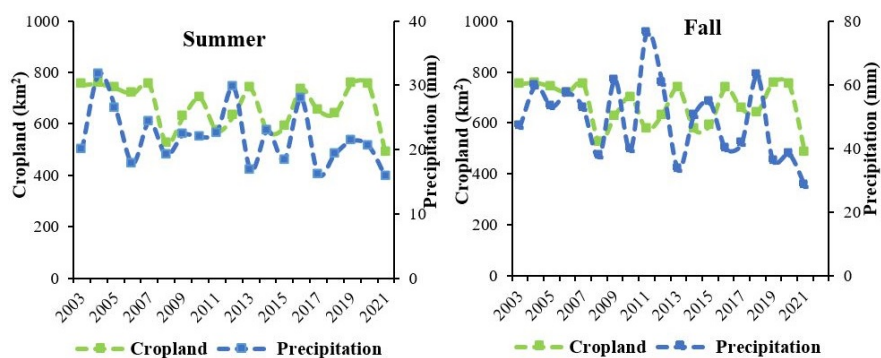


Figure 13. Time series of the total area of cropland with annual and seasonal precipitation.

Table 9. Correlation between annual EVI of cropland with seasonal and annual precipitation.

Precipitation	Winter	Spring	Summer	Fall	Annual
EVI	0.333 *	0.556 **	0.193	−0.111	0.532 **

* Denotes a significant correlation at $p = 0.05$ ** Denotes a significant correlation at $p = 0.01$.

4. Discussion

In this research, the dynamics of vegetation in relation to the detection and quantification of drought was investigated using remote sensing data in the Atrak basin for 2003–2021. According to the land use map (Figure 2), and as indicated in Table 3, which highlights that the vegetation cover classified as “poor” occupies the largest area, a huge part of the Atrak basin is covered by grasslands. Furthermore, as depicted in Figure 6, the vegetation anomaly has an increasing trend in the eastern parts of the basin and a slightly decreasing trend in the western parts of the basin, while in some specific areas, it is stable. The findings showed that the lowest vegetation area was observed in 2008 (4.89%), 2014 (5.75%), 2017 (6.81%), and 2021 (6.61%). According to the VCI index, 2008 was identified as the driest year, with a VCI of 95.9%, consistent with the findings of other studies [54]. Conversely, during the years with very high rainfall, such as 2004, 2007, 2009, and 2019, the vegetation coverage occupied 12.08%, 10.78%, 9.61%, and 18.25% of the total vegetation area, respectively. To some extent, vegetation cover follows the occurring rainfall pattern of change, with low rainfall years leading to decreased soil moisture, stress for vegetation, and, subsequently, reduced vegetation cover.

Based on the results of the VCI index, the highest occurrence of drought area occurred in the years 2008 (95.93%), 2011 (71.5%), 2014 (67.8%), 2017 (61.5%), and 2021 (57.6%), while the lowest drought area was recorded in 2010 (2.6%), 2013 (5.4%), 2016 (2%), 2019 (2.19%), and 2020 (9.7%). This result is in line with other studies’ conclusions [18,55]. Additionally, the Standardized Precipitation Index (SPI) has been employed to monitor drought conditions [56]. The SPI analysis indicates that the years 2004, 2007, 2009, and 2019 exhibited conditions ranging from moderately wet to very heavy wet, whereas the years 2008, 2014, and 2021 experienced moderate to severe drought conditions [27,57]. In 2010, 2016, and 2019 the highest percentage of vegetation area was observed. According to the Standardized Precipitation Index (SPI), 2019, with 227.5 mm of rainfall, is classified as a very wet year, and it exhibited the maximum vegetation coverage during this year, spanning an area of 14,404 km². Conversely, the lowest amount of rainfall in this season occurred in 2015, with 78.2 mm, while the minimum vegetation cover was in 2008, covering an area of 2776.6 km². It is worth noting that while rainfall is a crucial factor in vegetation changes, it may not always be the sole determining factor, as other factors such as soil texture and salinity can also play a role [49].

The conducted analyses demonstrate a significant relationship between precipitation and vegetation cover, which is also indicated by other authors [58,59]. This correlation indicates that changes in vegetation cover are somewhat influenced by the amount of

rainfall in the region, and these two factors have a linear and direct relationship with each other. This finding aligns with the results of previous studies [60–63]. However, our results also suggest a phase delay between precipitation and EVI cycles, with a relatively higher correlation observed between spring precipitation and summer EVI than spring precipitation and spring EVI. This observation aligns with the greening response typically occurring a few weeks after rainfall events. This was shown in one of the papers using the cross-wavelet analysis for eight eco-regions of Italy to show that the forested regions with higher altitudes had a positive correlation with almost in-phase annual coherency between NDVI and precipitation, while, for vegetation in the warmest eco-region, lowest annual coherencies between NDVI and precipitation were observed [64]. Additionally, a negative correlation between vegetation and temperature was observed, indicating another climatic factor influencing vegetation dynamics in the Atrak River basin. It is also worth noting that, similar to the observations in the referenced paper [64], we found that the correlations between EVI and LST were almost out of phase, with the highest correlation between spring LST and spring EVI, and relatively high correlations between summer LST and summer EVI. However, high correlations were also observed between spring LST and summer EVI, as well as spring EVI and summer LST, underscoring the complexity of the relationships between climatic variables and vegetation dynamics.

Furthermore, considering the critical role of agricultural lands in food security and the country's economy, the agricultural lands within the Atrak basin were separately investigated. The analysis indicates fluctuations in the extent of agricultural land over the study period, with some years witnessing larger agricultural areas compared to others. However, the majority of agricultural lands fall into the "very poor" and "poor" classes, underscoring the need for targeted interventions to improve soil fertility and agricultural productivity in the region. Additionally, a significant correlation was found between spring precipitation and cropland cover. Seasonal rainfall plays a crucial role in agriculture, influencing decisions such as the selection of seed species, the quantity of species to plant, and the timing of seed planting. A staggering 79% of farmers base their planting decisions on their predictions for the upcoming season's weather. Interestingly, approximately two-thirds of these predictions stem from past experiences, while the remaining third relies on observations from the previous season. However, a notable challenge arises from the lack of precise correlation between rainfall patterns in consecutive seasons, making accurate rainfall predictions difficult. Consequently, this uncertainty poses challenges for farmers in selecting appropriate seed varieties and drought-resistant cultivars. Ultimately, farmers' anticipations regarding future seasonal weather serve as a pivotal factor in guiding cropping decisions [65]. In semi-arid regions like the Atrak basin, where grasslands are prevalent, an annual rainfall range of 300–600 mm (mm) may be considered favorable for maintaining healthy grassland coverage, while, generally, for successful dry agriculture, regions may require annual rainfall ranging from 200 to 500 mm, with variations based on specific crop requirements and local conditions [66]. Sustainable management strategies should prioritize measures to mitigate the impact of droughts, enhance soil moisture retention, and improve the resilience of ecosystems and agricultural systems to climate variability. Additionally, integrated approaches that consider the complex interactions between climatic variables, land use practices, and vegetation dynamics are essential for fostering sustainable development and resilience in the region.

5. Conclusions

Understanding the factors that influence changes in vegetation cover is a critical aspect of vegetation management and protection. These factors encompass both climatic aspects and human-driven influences, such as management practices, human activities, restoration efforts, and exploitative actions. It is of great importance to elucidate the intricate relationship between these factors and the dynamics of vegetation, unraveling the mechanisms behind the changes. This study focused on understanding the factors impacting changes in vegetation cover, focusing on weather elements. Conducted in the

Atrak River basin from 2003 to 2021, the research employed satellite data and indices like VCI and SPI to analyze the connection between rainfall patterns and vegetation dynamics. The VCI helps identify drought and moisture levels, revealing trends over the years. Additionally, the SPI revealed years of moderate drought and normal conditions, with varying annual rainfall amounts.

Anomaly detection highlights rising vegetation trends in the eastern basin over time. The basin's vegetation cover varies, with poor vegetation being the largest category. Seasonally, spring sees the most extensive vegetation growth, particularly in 2010, 2016, and 2019. Contrasting vegetation distribution between the eastern and western halves is observed in summer and winter, with the eastern half displaying more scattered vegetation. The study established a notable correlation between spring precipitation and EVI in both spring and summer, indicating its significance. This emphasizes the pivotal role of spring precipitation in influencing vegetation dynamics within the Atrak basin area during the spring season. Additionally, in order to better understand the SPI in relation to vegetation dynamics, the LST index was used.

In conclusion, the findings of this study offer valuable insights for policymakers involved in vegetation management, water resource allocation, and environmental protection within the Atrak River basin. Our analysis of factors influencing vegetation cover, particularly focusing on weather elements, sheds light on the dynamics of the Atrak River basin's ecosystem. By utilizing advanced satellite imagery and indices, we established a clear correlation between rainfall patterns and vegetation dynamics, providing a data-driven understanding of how climatic shifts impact the region's vegetation health. While the identification of specific years marked by severe drought and abundant rainfall is crucial for policymakers, it is essential to note that addressing the predictability of droughts was beyond the scope of this study. However, acknowledging the limitations, our findings can still inform proactive measures during critical periods of water scarcity or excess. By understanding the intricate relationship between climatic factors and vegetation dynamics, policymakers can potentially mitigate the impacts of drought, support ecosystem restoration, and ensure the long-term sustainability of the region's environment and communities.

In summary, while our study does not delve into the predictability of droughts, it provides a foundation for informed decision making and resource allocation strategies, thus contributing to the overall resilience and well-being of the Atrak River basin.

Author Contributions: Conceptualization, I.R.; Data curation, I.R. and F.S.; Formal analysis, I.R. and F.S.; Investigation, I.R., F.S., E.R.M.V., A.S. and J.K.; Methodology, I.R.; Project administration, H.O. and J.K.; Resources, I.R. and F.S.; Software, I.R. and F.S.; Supervision, J.K.; Validation, I.R., F.S., H.O., E.R.M.V. and J.K.; Visualization, I.R.; Writing—original draft, I.R., F.S. and J.K.; Writing—review and editing, H.O., E.R.M.V., A.S. and J.K. All authors have read and agreed to the published version of the manuscript.

Funding: This work was supported by Vedurfelagid, Rannis and Rannsoknastofa i vedurfraedi.

Institutional Review Board Statement: Not applicable.

Informed Consent Statement: Not applicable.

Data Availability Statement: Data available after contacting Iman Rousta irousta@yazd.ac.ir.

Acknowledgments: Iman Rousta is deeply grateful to Haraldur Olafsson (Institute for Atmospheric Sciences-Weather and Climate, and Department of Physics, University of Iceland, and Icelandic Meteorological Office (IMO)), for his great support, kind guidance, and encouragement.

Conflicts of Interest: The authors declare no conflicts of interest. The funders had no role in the design of the study; in the collection, analyses, or interpretation of data; in the writing of the manuscript; or in the decision to publish the results.

References

- Peng, J.; Liu, Z.; Liu, Y.; Wu, J.; Han, Y. Trend analysis of vegetation dynamics in Qinghai–Tibet Plateau using Hurst Exponent. *Ecol. Indic.* **2012**, *14*, 28–39. [[CrossRef](#)]
- Gao, Q. Problems and Countermeasures of ecological management in Hanjiang River Basin. *Shaanxi Agric. Sci.* **2012**, *3*, 192–195.
- Mohseni, N.; Sepehr, A. Self-organized vegetation patterns: Early warning signals for predicting ecosystem transitions. *J. Environ. Stud.* **2015**, *41*, 163–177. [[CrossRef](#)]
- Huang, H.; Huang, J.; Wu, Y.; Zhuo, W.; Song, J.; Li, X.; Li, L.; Su, W.; Ma, H.; Liang, S. The Improved Winter Wheat Yield Estimation by Assimilating GLASS LAI into a Crop Growth Model with the Proposed Bayesian Posterior-Based Ensemble Kalman Filter. *IEEE Trans. Geosci. Remote Sens.* **2023**, *61*, 4401818. [[CrossRef](#)]
- Dastigerdi, M.; Nadi, M.; Sarjaz, M.R.; Kiapasha, K. Vegetation trend analysis using NDVI time series of Modis satellite in the northeast of Iran. *J. Water Soil Conserv.* **2022**, *29*, 135–150. [[CrossRef](#)]
- Pettorelli, N.; Vik, J.O.; Mysterud, A.; Gaillard, J.-M.; Tucker, C.J.; Stenseth, N.C. Using the satellite-derived NDVI to assess ecological responses to environmental change. *Trends Ecol. Evol.* **2005**, *20*, 503–510. [[CrossRef](#)]
- Qiu, S.; Yang, H.; Zhang, S.; Huang, S.; Zhao, S.; Xu, X.; He, P.; Zhou, W.; Zhao, Y.; Yan, N.; et al. Carbon Storage in an Arable Soil Combining Field Measurements, Aggregate Turnover Modeling and Climate Scenarios. *Catena* **2023**, *220*, 106708. [[CrossRef](#)]
- Moghim, J. *Introduction Some of Important Range Species, Suitable for Range Improvement in Iran*; Arvan Press: San Francisco, CA, USA, 2005; p. 669.
- Song, Y.; Ma, M. A Statistical Analysis of the Relationship between Climatic Factors and the Normalized Difference Vegetation Index in China. *Int. J. Remote Sens.* **2011**, *32*, 3947–3965. [[CrossRef](#)]
- Tan, S.Y. The Influence of Temperature and Precipitation Climate Regimes on Vegetation Dynamics in the US Great Plains: A Satellite Bioclimatology Case Study. *Int. J. Remote Sens.* **2007**, *28*, 4947–4966. [[CrossRef](#)]
- Katiraie-Boroujerdy, P.S. Comparison of high-resolution gridded monthly satellite and ground-based precipitation data over Iran. *Iran. J. Geophys.* **2016**, *7*, 149–160.
- Zhang, T.; Song, B.; Han, G.; Zhao, H.; Hu, Q.; Zhao, Y.; Liu, H. Effects of Coastal Wetland Reclamation on Soil Organic Carbon, Total Nitrogen, and Total Phosphorus in China: A Meta-Analysis. *Land Degrad. Dev.* **2023**, *34*, 3340–3349. [[CrossRef](#)]
- Yin, L.; Wang, L.; Li, T.; Lu, S.; Tian, J.; Yin, Z.; Li, X.; Zheng, W. U-Net-LSTM: Time Series-Enhanced Lake Boundary Prediction Model. *Land* **2023**, *12*, 1859. [[CrossRef](#)]
- Yin, L.; Wang, L.; Li, T.; Lu, S.; Yin, Z.; Liu, X.; Li, X.; Zheng, W. U-Net-STN: A Novel End-to-End Lake Boundary Prediction Model. *Land* **2023**, *12*, 1602. [[CrossRef](#)]
- Li, R.; Zhu, G.; Lu, S.; Sang, L.; Meng, G.; Chen, L.; Jiao, Y.; Wang, Q. Effects of Urbanization on the Water Cycle in the Shiyang River Basin: Based on Stable Isotope Method. *Hydrol. Earth Syst. Sci.* **2023**, *27*, 4437–4452. [[CrossRef](#)]
- Zhao, Y.; Wang, H.; Song, B.; Xue, P.; Zhang, W.; Peth, S.; Hill, R.L.; Horn, R. Characterizing Uncertainty in Process-Based Hydraulic Modeling, Exemplified in a Semiarid Inner Mongolia Steppe. *Geoderma* **2023**, *440*, 116713. [[CrossRef](#)]
- Guan, H.; Huang, J.; Li, L.; Li, X.; Miao, S.; Su, W.; Huang, H. Improved Gaussian Mixture Model to Map the Flooded Crops of VV and VH Polarization Data. *Remote Sens. Environ.* **2023**, *295*, 113714. [[CrossRef](#)]
- Mahmood, S.A.R.; Rousta, I.; Mazidi, A. Investigating the Sustainability of Vegetation Change Trends Using Remote Sensing (Case Study: Northern River Basin of Afghanistan). *Geogr. Environ. Sustain.* **2022**, *12*, 17–35. [[CrossRef](#)]
- Behrang-Manesh, M.; Khosravi, H.; Azarnivand, H.; Senatore, A. Quantifying the trend of vegetation changes using remote sensing (Case study: Fars Province). *J. Plant Ecosyst. Conserv.* **2020**, *7*, 295–318.
- Rousta, I.; Olafsson, H.; Moniruzzaman, M.; Zhang, H.; Liou, Y.-A.; Mushore, T.D.; Gupta, A. Impacts of Drought on Vegetation Assessed by Vegetation Indices and Meteorological Factors in Afghanistan. *Remote Sens.* **2020**, *12*, 2433. [[CrossRef](#)]
- Regmi, R.; Ma, Y.; Ma, W.; Baniya, B.; Bashir, B. Interannual Variation of NDVI, Precipitation and Temperature during the Growing Season in Langtang National Park, Central Himalaya, Nepal. *Appl. Ecol. Environ. Sci.* **2020**, *8*, 218–228. [[CrossRef](#)]
- Zhang, D.; Wu, F.; Fang, Y.; Lu, N. Spatial and Temporal Variation Trend Analysis of Vegetation Cover in Urban Agglomeration of Pearl River Delta from 2000 to 2015. *IOP Conf. Ser. Earth Environ. Sci.* **2020**, *615*, 012028. [[CrossRef](#)]
- Kazemzadeh, M.; Noori, Z.; Bayat, A.; Saedi Farkoush, S.; Elyasi, A.A.; Alipour, H.; Mansour Fallah, A. An Evaluation of the Effect of Natural and Human Factors on the Linear and Non-linear Changes in Vegetation Using the Landsat Images of the Khor-Sefidarak Watershed, the Province of Alborz. *Watershed Manag. Res. J.* **2021**, *34*, 95–114. [[CrossRef](#)]
- Gu, Z.; Zhang, Z.; Yang, J.; Wang, L. Quantifying the Influences of Driving Factors on Vegetation EVI Changes Using Structural Equation Model: A Case Study in Anhui Province, China. *Remote Sens.* **2022**, *14*, 4203. [[CrossRef](#)]
- Rousta, I.; Moniruzzaman, M.; Olafsson, H.; Zhang, H.; Baranowski, P.; Tkaczyk, P.; Lipińska, H.; Kępkowicz, A.; Krzyszcak, J. Investigation of the Vegetation Coverage Dynamics and its Relation to Atmospheric Patterns in Kabul River Basin in Afghanistan. *Pure Appl. Geophys.* **2022**, *179*, 3075–3094. [[CrossRef](#)]
- Jiao, Y.; Zhu, G.; Meng, G.; Lu, S.; Qiu, D.; Lin, X.; Sun, N. Estimating Non-Productive Water Loss in Irrigated Farmland in Arid Oasis Regions: Based on Stable Isotope Data. *Agric. Water Manag.* **2023**, *289*, 108515. [[CrossRef](#)]
- Rousta, I.; Mansourmoghaddam, M.; Olafsson, H.; Krzyszcak, J.; Baranowski, P.; Zhang, H.; Tkaczyk, P. Analysis of the recent trends in vegetation dynamics and its relationship with climatological factors using remote sensing data for Caspian Sea watersheds in Iran. *Int. Agrophys.* **2022**, *36*, 139–153. [[CrossRef](#)] [[PubMed](#)]

28. Rousta, I.; Olafsson, H.; Zhang, H.; Moniruzzaman, M.; Baranowski, P.; Krzyszcak, J. Anthropogenic Factors Affecting the Vegetation Dynamics in the Arid Middle East. *Environ. Clim. Technol.* **2022**, *26*, 774–805. [[CrossRef](#)]
29. Rousta, I.; Sharif, M.; Heidari, S.; Kiani, A.; Olafsson, H.; Krzyszcak, J.; Baranowski, P. Climatic Variables Impact on Inland Lakes Water Levels and Area Fluctuations in an Arid/Semi-Arid Region of Iran, Iraq, and Turkey Based on the Remote Sensing Data. *Earth Sci. Inf.* **2023**, *16*, 1611–1635. [[CrossRef](#)]
30. Nabizada, A.F.; Rousta, I.; Mozaffari, G.; Dalvi, M.; Olafsson, H.; Siedliska, A.; Baranowski, P.; Tkaczyk, P.; Krzyszcak, J. A remotely sensed study of the impact of meteorological parameters on vegetation for the eastern basins of Afghanistan. *Earth Sci. Inform.* **2023**, *16*, 1293–1312. [[CrossRef](#)]
31. Zhu, G.; Yong, L.; Zhao, X.; Liu, Y.; Zhang, Z.; Xu, Y.; Wang, L. Evaporation, Infiltration and Storage of Soil Water in Different Vegetation Zones in the Qilian Mountains: A Stable Isotope Perspective. *Hydrol. Earth Syst. Sci.* **2022**, *26*, 3771–3784. [[CrossRef](#)]
32. Barzali, M.; Azimi, M.; Abdolhosseini, M.; Lotfi, A. The Assessment of Rangeland Ecosystem Services in sediment retention via InVEST Model (Atrak Watershed, Golestan Province). *Iran. J. Range Desert Res.* **2022**, *29*, 133–144. [[CrossRef](#)]
33. Azimi, M.; Haghdadi, M.; Riyazinia, V.; Molnár, Z. Expert Understandings on Rangeland Ecosystem Services and Their Sustainable Management (Atrak River Basin, NE Iran). *Environ. Resour. Res.* **2020**, *8*, 109–120. [[CrossRef](#)]
34. Goli, A. *Political and Social History of the Turkmens*, 1st ed.; Alam Publication: Benguet, PI, USA, 1987; p. 22.
35. Hansen, M.C.; DeFries, R.S.; Townshend, J.R.; Sohlberg, R. Global land cover classification at 1 km spatial resolution using a classification tree approach. *Int. J. Remote Sens.* **2000**, *21*, 1331–1364. [[CrossRef](#)]
36. Belward, A.S.; Estes, J.E.; Kline, K.D. The IGBP-DIS global 1-km land-cover data set DISCover: A project overview. *Photogramm. Eng. Remote Sens.* **1999**, *65*, 1013–1020.
37. Friedl, M.A.; McIver, D.K.; Hodges, J.C.; Zhang, X.Y.; Muchoney, D.; Strahler, A.H.; Woodcock, C.E.; Gopal, S.; Schneider, A.; Cooper, A. Global land cover mapping from MODIS: Algorithms and early results. *Remote Sens. Environ.* **2002**, *83*, 287–302. [[CrossRef](#)]
38. Friedl, M.A.; Sulla-Menashe, D.; Tan, B.; Schneider, A.; Ramankutty, N.; Sibley, A.; Huang, X. MODIS Collection 5 global land cover: Algorithm refinements and characterization of new datasets. *Remote Sens. Environ.* **2010**, *114*, 168–182. [[CrossRef](#)]
39. Sulla-Menashe, D.; Friedl, M.A. *User Guide to Collection 6 MODIS Land Cover (MCD12Q1 and MCD12C1) Product*; USGS: Reston, VA, USA, 2018; pp. 1–18.
40. Li, B.; Tang, H.; Chen, D. Drought monitoring using the modified temperature/vegetation dryness index. In Proceedings of the 2009 2nd International Congress on Image and Signal Processing, Tianjin, China, 17–19 October 2009; pp. 1–5. [[CrossRef](#)]
41. Mansourmoghaddam, M.; Ghafarian Malamiri, H.R.; Rousta, I.; Olafsson, H.; Zhang, H. Assessment of Palm Jumeirah Island’s Construction Effects on the Surrounding Water Quality and Surface Temperatures during 2001–2020. *Water* **2022**, *14*, 634. [[CrossRef](#)]
42. McKee, T.B.; Doesken, N.J.; Kleist, J. The relationship of drought frequency and duration to time scales. In Proceedings of the 8th Conference on Applied Climatology, Anaheim, CA, USA, 17–22 January 1993; pp. 179–184.
43. Kogan, F.N. Droughts of the late 1980s in the United States as derived from NOAA polar-orbiting satellite data. *Bull. Am. Meteorol. Soc.* **1995**, *76*, 655–668. [[CrossRef](#)]
44. Kogan, F.N. Global drought watch from space. *Bull. Am. Meteorol. Soc.* **1997**, *78*, 621–636. [[CrossRef](#)]
45. Zhao, W.; He, J.; Wu, Y.; Xiong, D.; Wen, F.; Li, A. An analysis of land surface temperature trends in the central Himalayan region based on MODIS products. *Remote Sens.* **2019**, *11*, 900. [[CrossRef](#)]
46. Wu, Y.; Onipchenko, V. The impact of snow-cover on alpine vegetation type of different aspects in the west of Sichuan Province. *Shengtai Xuebao. Acta Ecol. Sin.* **2007**, *27*, 5120–5129.
47. Zhou, H.; Deng, Z.; Xia, Y.; Fu, M. A new sampling method in particle filter based on Pearson correlation coefficient. *Neurocomputing* **2016**, *216*, 208–215. [[CrossRef](#)]
48. Lee Rodgers, J.; Nicewander, W.A. Thirteen ways to look at the correlation coefficient. *Am. Stat.* **1988**, *42*, 59–66. [[CrossRef](#)]
49. Dastorani, M.; Komaki, C.B.; Khosravi, H.; Ghelichipour, Z. Investigation of the trend of rainfall and vegetation changes in arid and semiarid regions (Case Study: Khorasan Razavi, Iran). *J. Arid Biome.* **2019**, *9*, 11–19.
50. Karnieli, A.; Agam, N.; Pinker, R.T.; Anderson, M.; Imhoff, M.L.; Gutman, G.G.; Panov, N.; Goldberg, A. Use of NDVI and Land Surface Temperature for Drought Assessment: Merits and Limitations. *J. Clim.* **2010**, *23*, 618–633. [[CrossRef](#)]
51. Elsen, P.R.; Kalyanaraman, R.; Ramesh, K.; Wilcove, D.S. The importance of agricultural lands for Himalayan birds in winter. *Conserv. Biol.* **2017**, *31*, 416–426. [[CrossRef](#)] [[PubMed](#)]
52. Elame, F.; Doukkali, R.; Lionboui, H. Dynamic modeling of climate change impact on agricultural lands and water resources. In *Handbook of Climate Change Management*; Springer: Berlin/Heidelberg, Germany, 2020; pp. 1–21. [[CrossRef](#)]
53. Tun-Oo, A.; Van Huylenbroeck, G.; Speelman, S. Measuring the Economic Impact of Climate Change on Crop Production in the Dry Zone of Myanmar: A Ricardian Approach. *Climate* **2020**, *8*, 9. [[CrossRef](#)]
54. Zargarani, P.; Bazrafshan, J.; Aghashariatmadary, Z.; Hejabi, S.; Kamali, S. Daily Monitoring of Drought Effects on Vegetation Cover Using ERA-Interim Precipitation Data and MODIS Images (Case Study: Kermanshah Province). *J. Agric. Meteorol.* **2020**, *7*, 3–14. [[CrossRef](#)]
55. Razipoor, M.E. Assessing the vegetation Condition of Herat Province, Afghanistan Using GIS. *Appl. Geol. Geophys.* **2019**, *7*, 92–97. [[CrossRef](#)]

56. Baaghideh, M.; Alijani, B.; Ziaeean, P. Investigating the possibility of using NDVI vegetation index in drought analysis in Isfahan province. *J. Geogr. Stud. Arid Reg.* **2011**, *1*, 1–16.
57. Firouzi, F.; Tavosi, T.; Mahmoudi, P. Investigating the statistical relationship between climatic and hydrological variables with Vegetation Dynamics in a dry climate (Case study: Sistan plain in eastern Iran). *Desert Manag.* **2018**, *6*, 99–111. [[CrossRef](#)]
58. Birtwistle, A.N.; Laituri, M.; Bledsoe, B.; Friedman, J.M. Using NDVI to measure precipitation in semi-arid landscapes. *J. Arid Environ.* **2016**, *131*, 15–24. [[CrossRef](#)]
59. Shi, L.; Fan, H.; Yang, L.; Jiang, Y.; Sun, Z.; Zhang, Y. NDVI-Based Spatial and Temporal Vegetation Trends and Their Response to Precipitation and Temperature Changes in the Mu Us Desert from 2000 to 2019. *Water Sci. Technol.* **2023**, *88*, 430–442. [[CrossRef](#)] [[PubMed](#)]
60. Tucker, C.J.; Vanpraet, C.L.; Sharman, M.; Van Ittersum, G. Satellite Remote Sensing of Total Herbaceous Biomass Production in the Senegalese Sahel: 1980–1984. *Remote Sens. Environ.* **1985**, *17*, 233–249. [[CrossRef](#)]
61. Malo, A.R.; Nicholson, S.E. A study of rainfall and vegetation dynamics in the African Sahel using normalized difference vegetation index. *J. Arid Environ.* **1990**, *19*, 1–24. [[CrossRef](#)]
62. Schultz, P.; Halpert, M. Global Correlation of Temperature, NDVI, and Precipitation. *Adv. Space Res.* **1993**, *13*, 277–280. [[CrossRef](#)]
63. Yang, L.; Wylie, B.K.; Tieszen, L.L.; Reed, B.C. An Analysis of Relationships among Climate Forcing and Time-Integrated NDVI of Grasslands over the US Northern and Central Great Plains. *Remote Sens. Environ.* **1998**, *65*, 25–37. [[CrossRef](#)]
64. Ghaderpour, E.; Mazzanti, P.; Mugnozsa, G.S.; Bozzano, F. Coherency and Phase Delay Analyses between Land Cover and Climate across Italy via the Least-Squares Wavelet Software. *Int. J. Appl. Earth Obs. Geoinf.* **2023**, *118*, 103241. [[CrossRef](#)]
65. Guido, Z.; Zimmer, A.; Lopus, S.; Hannah, C.; Gower, D.; Waldman, K.; Krell, N.; Sheffield, J.; Caylor, K.; Evans, T. Farmer Forecasts: Impacts of Seasonal Rainfall Expectations on Agricultural Decision-Making in Sub-Saharan Africa. *Clim. Risk Manag.* **2020**, *30*, 100247. [[CrossRef](#)]
66. Azimi, M.; Barzali, M.; Abdolhosseini, M.; Lotfi, A. Examining the Impact of Rangeland Condition on Water Conservation by Using an Integrated Modelling Approach. *Land Degrad. Dev.* **2020**, *32*, 3711–3719. [[CrossRef](#)]

Disclaimer/Publisher’s Note: The statements, opinions and data contained in all publications are solely those of the individual author(s) and contributor(s) and not of MDPI and/or the editor(s). MDPI and/or the editor(s) disclaim responsibility for any injury to people or property resulting from any ideas, methods, instructions or products referred to in the content.